Atmospheric
Chemistry
and Physics
Discussions

Open Access

On the effectiveness of nitrogen oxide reductions as a control over ammonium nitrate aerosol

S. E. Pusede[1,a], K. C. Duffey[1], A. A. Shusterman[1], A. Saleh[1], J. L. Laughner[1],
P. J. Wooldridge[1], Q. Zhang[2], C. L. Parworth[2], H. Kim[3], S. L. Capps[4], L. C. Valin[5],
C. D. Cappa[6], A. Fried[7], J. Walega[7], J. B. Nowak[8], R. M. Hoff[9], T. A. Berkoff[10],
A. J. Beyersdorf[10], J. Olson[10], J. H. Crawford[10], and R. C. Cohen[1,11]

[1]Department of Chemistry, University of California Berkeley, Berkeley, CA, 94720, USA
[2]Department of Environmental Toxicology, University of California at Davis, Davis, CA, 95616, USA
[3]Center for Environment, Health and Welfare Research, Korea Institute of Science and Technology, Seoul, Korea
[4]Department of Mechanical Engineering, University of Colorado Boulder, Boulder, CO, 80309, USA
[5]Lamont-Doherty Earth Observatory, Columbia University, Palisades, NY, 10964, USA
[6]Department of Civil and Environmental Engineering, University of California at Davis, Davis, CA, 95616, USA
[7]Institute of Arctic and Alpine Research, University of Colorado, Boulder, CO, 80309, USA

Title Page

Abstract	Introduction
Conclusions	References
Tables	Figures

|◄ | ►|
◄ | ►

Back | Close

Full Screen / Esc

Printer-friendly Version

Interactive Discussion

[8]Aerodyne Research, Inc., Billerica, MA, 01821, USA

[9]Department of Physics, University of Maryland Baltimore County, Baltimore, MD, 21250, USA

[10]NASA Langley Research Center, Hampton, VA, 23681, USA

[11]Department of Earth and Planetary Science, University of California Berkeley, Berkeley, CA, 94720, USA

[a]now at: Department of Environmental Sciences, University of Virginia, Charlottesville, VA, 22904, USA

Correspondence to: R. C. Cohen (rccohen@berkeley.edu)

Discussion Paper | Discussion Paper | Discussion Paper | Discussion Paper | Discussion Paper |

ACPD

15, 27087–27136, 2015

NO$_x$ control over ammonium nitrate

S. E. Pusede et al.

Title Page

Abstract | Introduction

Conclusions | References

Tables | Figures

|◀ | ▶|

◀ | ▶

Back | Close

Full Screen / Esc

Printer-friendly Version

Interactive Discussion

Abstract

Nitrogen oxides (NO$_x$) have fallen steadily across the US over the last fifteen years. At the same time, due to patterns diesel truck activities, NO$_x$ concentrations decrease on weekends relative to weekdays, largely without co-occurring changes in other gas-phase emissions. These trends taken together provide two independent constraints on the role of NO$_x$ in the nonlinear chemistry of atmospheric oxidation. In this context, we interpret interannual trends in wintertime ammonium nitrate (NH$_4$NO$_3$) in the San Joaquin Valley of California, a location with the worst aerosol pollution in the US and where a large portion of aerosol mass is NH$_4$NO$_3$. Here, we show that NO$_x$ reductions have simultaneously decreased nighttime and increased daytime NH$_4$NO$_3$ production over the last decade. We find a substantial decrease in NH$_4$NO$_3$ since 2000 and conclude that this decrease is due to reduced nitrate radical-initiated production at night in residual layers that are decoupled from fresh emissions at the surface. Further reductions in NO$_x$ are imminent in California, and nationwide, and we make a quantitative prediction of the response of NH$_4$NO$_3$. We show that the combination of rapid chemical production and efficient NH$_4$NO$_3$ loss via deposition of gas-phase nitric acid implies high aerosol days in cities in the San Joaquin Valley air basin are responsive to local changes in NO$_x$ within those individual cities. Our calculations indicate that large decreases in NO$_x$ in the future will not only lower wintertime NH$_4$NO$_3$ concentrations, they will also cause a transition in the dominant NH$_4$NO$_3$ source from nighttime to daytime chemistry.

1 Introduction

Aerosol abundances are decreasing across the US, improving air quality and affecting climate. These decreases have been broadly attributed to regulatory controls on the emissions of gas-phase precursors; however, it has proven difficult to link precursor

reductions to observed changes in aerosol concentration via specific chemical mechanisms. Thus, there is little knowledge of how impacts will scale in the future.

We present an analysis to identify driving chemical mechanisms and to quantify the effects of large reductions in nitrogen oxides (NO_x) (Russell et al., 2012; McDonald et al., 2012) on secondary aerosol chemistry. We take advantage of decreased NO_x emissions on weekends compared to weekdays, which occur mostly without changes in other gas-phase emissions (Dallmann et al., 2012), and couple these weekday-weekend patterns to long-term NO_x reductions (Pusede and Cohen, 2012). The effect is that weekday NO_x levels equal weekend NO_x years earlier in the record (Fig. 1). We use this NO_x constraint to interpret trends in observed wintertime ammonium nitrate (NH_4NO_3) concentrations over the last decade in the San Joaquin Valley (SJV) of California.

The SJV experiences the most severe aerosol pollution in the US (American Lung Association, 2014). From 2001–2013 there were on average 44 exceedances each winter (November–March) of the 24 h national ambient air quality standard (NAAQS) of $35\,\mu g\,m^{-3}$ in Bakersfield and Fresno, with as many as 70 per winter early in the record. High aerosol in the SJV is generally limited to the winter months, with few exceedances occurring in other seasons. In the SJV, 30–80 % of wintertime aerosol mass is NH_4NO_3 and the remaining portion is largely organic material (Chow et al., 2006; Chen et al., 2007; Ge et al., 2012). Characteristics of the wintertime SJV that are conducive to high aerosol abundances include: shallow boundary layers (Bianco et al., 2011); prolonged periods of stagnation (Smith et al., 1981); and large emissions of NO_x ($NO_x \equiv NO + NO_2$), ammonia (NH_3) (Goebes et al., 2003; Clarisse et al., 2010), and organic aerosol (Ge et al., 2012). These conditions pose challenges to accurately simulating secondary aerosol in the region, as models need to represent bidirectional NH_3 exchange (Gilliland et al., 2006; Flechard et al., 2010; Pleim et al., 2013), variable local meteorology, complex airflow, and vertical stratification in the rates of NO_2 oxidation to NO_3^- (Heald et al., 2012; Walker et al., 2012; Kelly et al., 2014; Schiferl et al., 2014).

In this paper, we take an observational approach, combining the decade-long record of speciated aerosol concentrations and of gas-phase precursors in the region with detailed measurements collected during the DISCOVER-AQ experiment (Deriving Information on Surface Conditions from COlumn and VERtically resolved observations relevant to Air Quality, 14 January–14 February 2013). We show that wintertime NO_3^-, which we treat as a measured surrogate for NH_4NO_3, has been dependent only on the NO_2 concentration over the last twelve years. We calculate observationally-constrained nighttime and photochemical NO_3^- production rates and show that measured trends in wintertime NO_3^- can be explained by decreased nitrate radical-initiated production in nocturnal residual layers, which are unmonitored layers of the atmosphere that are effectively separated from surface emissions at night. We test the impacts of forthcoming NO_x emission controls on the probability of future NAAQS exceedances, showing that NO_x reductions will not only decrease the frequency of high aerosol days, but will also switch both the timing and the oxidation mechanisms that drive NH_4NO_3 production.

2 Results from observations

Trends in wintertime (November–March) 24 h NO_3^- vs. daytime (10 a.m.–3 p.m. LT) NO_2 are shown in Fig. 2 in the cities Fresno and Bakersfield on weekdays and weekends for the period 2001–2013. The source of these observations, the methods used for collection, and measurement biases are discussed in Appendix A. Weekdays are defined as Tuesday–Friday and weekends are Saturday–Sunday. We expect carryover to have some effect on the interpretation, as concentrations of NO_2 and aerosol are not only influenced by present day processes but also have some memory of processes occurring on the preceding day, especially in the winter when surface winds are slow and disorganized and horizontal transport is weak. We exclude Monday from weekdays for this reason but retain Saturdays to improve weekend statistics. As a result, weekend medians reported here might be slightly higher than would be observed due to weekend emissions alone. We define the day as beginning and ending at sunrise since

nighttime NO_3^- production builds from reactants present in the atmosphere during the preceding daytime hours. On any individual winter day, air stagnation and the planetary boundary layer (mixing) height are the dominant controls over gas and aerosol concentrations; however, considering the data separately by weekday and weekend and then comparing year-to-year changes, instead draws attention to the effects of emissions and subsequent chemistry.

The NO_3^- mass concentration is observed to depend explicitly on the previous day's daytime NO_2 concentration, with a sensitivity of $0.5\,\mu g\,m^{-3}\,ppb^{-1}$ NO_2 in Fresno and $0.64\,\mu g\,m^{-3}\,ppb^{-1}$ NO_2 in Bakersfield (slopes in Fig. 2). Since NO_2 has also decreased over the last decade, there is a corresponding interannual decrease in NO_3^-. Uncertainties in the NO_3^- concentration are computed as counting errors, with N as the total number of wintertime data points (3 year average), and are ±20 % on weekdays and ±30 % on weekends. Errors in NO_2 are computed in the same way and are less than ±9 % on weekdays and ±13 % on weekends in both Fresno and Bakersfield. One ppb NO_2 corresponds to $2.56\,\mu g\,m^{-3}$ NO_3^- after oxidation (at 25 °C and 1 atm), thus the observed correlation corresponds to a decrease in NO_3^- mass that is 20 % of the NO_2 decrease. We interpret the positive x-intercept in Fig. 2 as consistent with the known low bias in NO_3^- measurements (Appendix A) and the shorter wintertime atmospheric lifetime of NO_3^- than NO_2 (Sect. 4). Uncertainty estimates, including a low measurement bias of 25 % NO_3^-, are $\mu g\,m^{-3}\,ppb^{-1}$ NO_2 on weekdays and $\mu g\,m^{-3}\,ppb^{-1}$ NO_2 on weekends.

The key mechanistic information observed in Fig. 2 is that present day NO_3^- concentrations on weekdays are equal to what were observed on weekends a decade ago, i.e. the NO_2 dependence of NO_3^- is unchanged with time. From this, we conclude that the only source of NO_3^- in the atmosphere is oxidation of NO_2 and that agreement of NO_3^- in different years at identical NO_2 suggests there has been little change in the chemical mechanism producing NO_3^-, and hence NH_4NO_3.

Additional insight comes from observations made during DISCOVER-AQ, in which the sum of gas-phase nitric acid and aerosol-phase NO_3^- ($NO_{3\,(g+p)}^-$) was measured onboard the NASA P-3B on six research flights with almost identical flight patterns (Fig. 3a). See Appendix A for a description of the $NO_{3\,(g+p)}^-$ measurements and for the DISCOVER-AQ experiment. A comparison of the spatial distribution of $NO_{3\,(g+p)}^-$ within the fully developed (afternoon) boundary layer (see Appendix A for the boundary layer filtering procedure) and that of NO_2 observed from the satellite (Fig. 1) and NO_x from onboard the P3-B (Fig. 3b), suggests that $NO_{3\,(g+p)}^-$ better follows spatial patterns in NO_2 than gas-phase NH_3 (Fig. 3c), which is the precursor of particulate-phase NH_4^+. As is evident from Fig. 3a, urban-rural gradients in $NO_{3\,(g+p)}^-$ are steep. For example, in Bakersfield, $NO_{3\,(g+p)}^-$ was on average 18–20 $\mu g\,m^{-3}$ near the city center, which was twice as high as just 20 km to the northeast. Also inconsistent with observed spatial patterns is the transport of NH_4NO_3 from outside the central SJV. Typical daytime (10 a.m.–3 p.m. LT) winter wind speeds are ~ 2–$3\,m\,s^{-1}$; morning (6 a.m.–10 a.m. LT) winds are slower at ~ 1–$2\,m\,s^{-1}$ and nighttime winds are near zero. An air parcel moving at $3\,m\,s^{-1}$ would require approximately ~ 20 daytime h (multiple days) to reach Fresno from the upwind cities of Stockton or San Jose or travel from Fresno of Bakersfield.

We infer from Figs. 2 and 3 that the oxidation of locally emitted NO_x is the single largest term affecting the production of NH_4NO_3 and that transport and mixing are too slow to homogenize the aerosol throughout the wintertime SJV.

3 Chemistry in the dynamic near-surface atmosphere

Under the high NH_3, low sulfur dioxide, and high aerosol surface area conditions found in the SJV, NH_4NO_3 abundances are driven by NO_3^- production (PNO_3^-) and temperature. During the winter, it is cold enough that most NO_3^- is aerosol bound in the 24 h

average; thus, $P\text{NO}_3^-$ is rate limiting. $P\text{NO}_3^-$ occurs by distinct nighttime and daytime mechanisms, each of which is a nonlinear function of NO_2.

Nitrate radical (NO_3) is the most important nighttime oxidant (Brown and Stutz, 2012). It is formed via reaction of NO_2 with O_3 (Reaction R1).

5    $\text{NO}_2 + \text{O}_3 \rightarrow \text{NO}_3$ (R1)

NO_3-initiated chemistry occurs mainly at night because NO_3 photolyzes rapidly to NO_2. After sunset, large NO emissions can titrate O_3, altering the relative amounts of NO_2 and O_3, but conserving odd oxygen ($\text{O}_x \equiv \text{NO}_2 + \text{O}_3$). NO_3 radical production is a non-linear function of NO_2 for a given O_3 concentration, increasing with NO_2 at low NO_x, 10   maximizing when NO_2 is equal to O_3 at constant O_x, and decreasing at higher NO_x, shown as NO_2 (Appendix B, Fig. B1a).

In the evening, reduced sunlight diminishes the heating of the Earth's surface, leading to strong suppression of vertical mixing and the formation of a shallow nocturnal boundary layer (NBL). Between the NBL and the free troposphere, in the nocturnal 15   residual layer (NRL), mixing is weak and further layering may occur (Brown et al., 2007). The initial concentrations of species in the NRL are determined by the concentrations observed at the point when the residual layer decouples from the NBL, around sunset. Afterwards, the strong surface inversion keeps fresh emissions from entering the NRL. The NRL is seen by surface monitors in the morning when solar heating and 20   turbulent mixing reincorporate what was the NRL into the growing daytime boundary layer (Fig. 4), a process that also alters the NRL composition. On nights when NO_3 radical production in the NBL is zero due to high NO emissions, NO_3 chemistry may still be active in the dynamically decoupled NRL. Figure A1 (Appendix A) shows an example of at least two elevated $\text{NO}_{3\,(g+p)}^-$ residual layers observed during DISCOVER-AQ. 25   Loss from the atmosphere is likewise affected by this vertical structuring, as deposition to the surface occurs during the daytime and during the night from the NBL, but not during the night from the NRL.

Nitrate radical reacts with NO_2 to form dinitrogen pentoxide (N_2O_5) and generally in the atmosphere $N_2O_5 \gg NO_3$ (Brown et al., 2009; Brown and Stutz, 2012). The lifetime of N_2O_5 back to thermal decomposition to NO_2 and NO_3 is ~ 10 min at 270 K. NO_3 is also lost to reaction with certain organic species, especially compounds with unsatu-

5   rated carbon-carbon bonds. When reaction times are long, for example during long, dark winter nights, and when unsaturated hydrocarbon emissions are low, the most important loss of NO_3 is via N_2O_5 uptake onto aerosols (e.g., Dentener and Crutzen, 1993; Macintyre and Evans, 2010; Wagner et al., 2013), whereupon N_2O_5 reacts heterogeneously with aerosol-phase water to give two NO_3^-. The heterogeneous loss rate

10   of N_2O_5 is a function of the total aerosol surface area and of the fraction of gas-particle collisions resulting in N_2O_5 uptake, which is composition dependent, being inversely proportional to NO_3^- and dependent on the amount of organic aerosol (Brown et al., 2007; Bertram et al., 2009; Bertram and Thornton, 2009).

During the daytime, nitric acid (HNO_3) is the gas-phase reaction product of the oxida-

15   tion of NO_2 and the hydroxyl radical (OH) (Reaction R2). The production rate of HNO_3 increases rapidly with increasing NO_x at low NO_x and converges at a limit set by the primary HO_x ($HO_x \equiv OH + HO_2 + RO_2$) production rate at higher NO_x. The functional form of the dependence of HNO_3 production on NO_2 (Fig. B1b) arises from the non-linear effects of NO_x on the OH abundance, as NO_x both propagates and terminates

20   the HO_x catalytic cycle. Under the high NO_x conditions of the wintertime SJV, HNO_3 is the dominant daytime HO_x termination product. Combined with high NH_3, partitioning to the aerosol phase is a function of ambient temperature and humidity.

$$NO_2 + OH + M \rightarrow HNO_3 + M \tag{R2}$$

Trends in calculated wintertime PNO_3^- for the nighttime and daytime mechanisms, as

25   constrained by the observations (calculations and data are described in Appendix B), show that PNO_3^- in the NRL is the only chemistry that matches trends in NO_3^- (Fig. 2). Specifically, PNO_3^- in the NRL is the only chemistry that exhibits identical NO_2 dependence as observed in the NO_3^- measurements – both over time and from weekday

NO_x control over ammonium nitrate

S. E. Pusede et al.

Title Page

Abstract	Introduction
Conclusions	References
Tables	Figures

◄◄   ►►

◄   ►

Back   Close

Full Screen / Esc

Printer-friendly Version

Interactive Discussion

to weekend. In Fig. 5, the calculated annual wintertime daily-integrated $P\text{NO}_3^-$ in the NRL is shown vs. daytime NO_2 on weekdays and weekends in Fresno and Bakersfield. We compute that $P\text{NO}_3^-$ in the NRL has decreased by $\sim 1\,\mu\text{g}\,\text{m}^{-3}\,\text{day}^{-1}\,\text{ppb}^{-1}\,\text{NO}_2$ in both cities, approximately twice the trend observed in NO_3^- vs. NO_2. The total daytime

5 source (R2) has, by contrast, not significantly changed as a function of NO_2. $P\text{NO}_3^-$ attributed to the HO_x sources $\text{O}(^1\text{D}) + \text{H}_2\text{O}$ and formaldehyde (CH_2O) has slightly increased ($\sim 5\,\%$) since 2001 and that attributed to the HO_x source nitrous acid (HONO) has decreased almost equivalently (Appendix B, Fig. B2). In the NBL (not shown), as a result of reduced titration of O_3 at sunset, $P\text{NO}_3^-$ has increased from < 1 to 5–

10 $8\,\mu\text{g}\,\text{m}^{-3}\,\text{day}^{-1}$ on weekdays and to $10\text{–}13\,\mu\text{g}\,\text{m}^{-3}\,\text{day}^{-1}$ on weekends, that said, this increase has occurred within a volume only a fraction of the size of the NRL or of the daytime boundary layer.

4 Discussion

4.1 Relating concentration and production

15 The concentration of $\text{NO}_{3\,(g+p)}^-$ is a function of $P\text{NO}_3^-$, as well as loss and mixing. While high aerosol days in the SJV are in part attributed to persistent and severe stagnation, controls over the portion of aerosol mass that is NH_4NO_3 are far more dynamic (Pandis and Seinfeld, 1990; Vayenas et al., 2005). In this section we show that the effects of loss and mixing on the NO_3^- concentration are consistent with observed NO_3^- trends over

20 time, differences by day-of-week, accumulation rates during stagnation, and differences between Fresno and Bakersfield.

On days when NH_4NO_3 exceeded $20\text{–}30\,\mu\text{g}\,\text{m}^{-3}$, as measured from the ground in Fresno during DISCOVER-AQ, and as was typical during stagnation periods, the diurnal variability of NO_3^- at the surface was characterized by a steep and substantial in-

25 crease in NO_3^- in the morning, a slow decline through midday, and a rapid decrease in

the afternoon (Fig. 6). On these mornings, the rate of the rise in NO_3^- is consistent with reincorporation of high-NO_3^- NRL air into the boundary layer. At midday, OH-initiated PNO_3^-, atmospheric loss, and daily maximum winds all play upon [NO_3^-]. In the afternoon, OH-initiated PNO_3^- is minimal due to attenuated evening radiation (nocturnal PNO_3^- is then $\sim$ zero). On days exhibiting this pattern, the NO_3^- concentration was observed to decrease at a rate equal to $3.0 \pm 1.3 \, \mu g \, m^{-3} \, h^{-1}$ (1σ variability), with individual rates determined as the slopes of linear fits through the magenta data and identified as periods of steady decrease at least 3 h long. Time windows were allowed to vary, and the average window was 1:25 p.m.–4:05 p.m. LT, spanning 10:30 a.m.–6:30 p.m. LT. In what follows, we use this afternoon rate of change (when loss dominates production and mixing) to derive the atmospheric NO_3^- lifetime ($\tau_{NO_3^-}$).

The atmospheric lifetime of aerosol in the boundary layer is determined by wet and dry deposition of aerosol, the wet and dry deposition of gases in equilibrium with aerosol, and mixing to the free troposphere where concentrations are much lower. Wet deposition occurs by interaction with rain, which scavenges aerosol and soluble gases, and leaves the valley relatively clear. Multiday fog is common in the winter in the SJV (Holets and Swanson, 1981), enhancing NH_4NO_3 removal when fog leads to rain or drizzle (Jacob et al., 1986a, b), as inorganic ions readily partition into aqueous fog droplets (Waldman et al., 1982; Munger et al., 1983), but having little effect if fog dissipates. Fog has not been seen to accelerate the conversion of NO_2 to NO_3^- in the SJV (Jacob et al., 1984).

There are few direct measurements of deposition rates of aerosol, HNO_3, and NH_3. HNO_3 is theorized to deposit at a transport-limited rate, NH_3 exchange is dependent on surface and meteorological conditions, and aerosol, especially smaller particles, to deposit slowly. PM_1 to $PM_{2.5}$ deposition velocities (υ_d) have been reported to be 0.01 to $0.1 \, cm \, s^{-1}$ (Sehmel, 1980; Slinn, 1982), too slow to account for the observed afternoon loss rates in Fig. 6. To compute NO_3^- loss by deposition of gas-phase HNO_3, $HNO_{3(g)}$ was modeled with ISORROPIA II (Nenes et al., 1998; Fountoukis and Nenes, 2007) run

in forward mode, an approximation that was reasonable as (a) during the wintertime, temperatures were low and humidities were high and (b) NO_3^- was shown to be limiting to NH_4NO_3 (Fig. 2). ISORROPIA II was initialized as $[NO_3^- + HNO_3] = [NO_3^-]_{AMS}$ and $[NH_4^+ + NH_3] = [NH_4^+]_{AMS}$. Calculated $HNO_{3(g)}$ was added back to $[NO_3^- + HNO_3]$, while $NH_{3(g)}$ was added as 1.1 $HNO_{3(g)}$ (by mole) to ensure NH_3 was in excess. ISORROPIA II was solved iteratively until daytime $HNO_{3(g)}$ changed by < 2 % by mass. The phase state was set as metastable (e.g., Rood et al., 1989; Zhang et al., 2003; Vayenas et al., 2005). We assume that gases and aerosol are in equilibrium, that aerosols are homogenous and internally mixed, and that unaccounted-for factors do not influence the thermodynamics of the system (Vayenas et al., 2005). Calculated HNO_3 mixing ratios were greatest in the afternoon (12–4 p.m. LT), at which time they were 2 ppb on average for the DISCOVER-AQ time period and up to 4–6 ppb on the warm days only. In the 24 h average, $HNO_{3(g)}$ was 15 % of $[NO_3^- + HNO_3]$ by mass and was 40 % (median) in the afternoon. High $HNO_{3(g)}$ was generally simultaneous with the magenta-highlighted NO_3^- data (Fig. 6).

To compute the υ_d of HNO_3, the equation $\frac{\partial NO_3^-}{\partial t} = \frac{\upsilon_d}{h} C$ was solved, with $\frac{\partial NO_3^-}{\partial t}$ equal to the observed afternoon loss rate on designated (magenta) days, C equal to the daily mean $HNO_{3(g)}$ over the same time windows, and h equal to the maximum boundary layer height (i.e. the afternoon height) visually estimated according to aerosol backscatter estimates by a micro-pulse lidar supplemented with a wide-field receiver system (Appendix A). In this way, we derived υ_d equal to $5 \pm 2 \, \mathrm{cm \, s^{-1}}$, which was in line with previous direct measurements of 1–$10 \, \mathrm{cm \, s^{-1}}$ (e.g., Huebert and Robert, 1985; Meyers et al., 1989; Sievering et al., 2001; Volpe Horii et al., 2005; Farmer et al., 2006) and constrained estimates of $6 \, \mathrm{cm \, s^{-1}}$ (Vayenas et al., 2005). Given a υ_d of $5 \, \mathrm{cm \, s^{-1}}$ (assumed constant), the hourly $\frac{\partial NO_3^-}{\partial t}$ was computed for every hour of the day, with C equal to the time-varying $HNO_{3(g)}$ and h equal to the time-varying boundary layer height. For the daily time-varying h: the NBL was 10 % the maximum daytime boundary layer height, the morning increase occurred linearly over 5 h, the boundary layer

was fully developed at 11 a.m., and the evening (6 p.m.) collapse (also linear) took only 2 h.

With respect to surface deposition alone, $\tau_{NO_3^-}$ was calculated to be only 3 h (0.1 days) under daytime conditions. As a lower bound, if the true υ_d was at the slowest end of previous observations (1 cm s^{-1}), then $\tau_{NO_3^-}$ would be 14 h under daytime conditions. Lifetimes in this range are shorter than typical stagnation periods, observed to be 5 ± 1.5 days (1σ variability) in both Fresno and Bakersfield (decadal average). By comparison, $PM_1-PM_{2.5}$ υ_d yield $\tau_{NO_3^-}$ of 6–58 days. Such long lifetimes indicate the frequency of frontal passages controls the PM lifetime. Because the loss of NH_4NO_3, via HNO_3 deposition, is rapid and PNO_3^- is relatively large, high aerosol days are expected to be more responsive to changes in emissions than expected if one considered loss only through particle deposition.

There are other observational constraints that any account of aerosol NO_3^- in the SJV should explain. Median NO_3^- (2001–2013) is 25 % higher in Bakersfield than Fresno (Fig. 2). However, the observationally-constrained calculated total PNO_3^- (NRL plus OH-initiated) is 25 % lower in Bakersfield than Fresno (Fig. 5). We find that wintertime stagnation events, defined as continuous days with increasing 24 h $PM_{2.5}$, are more severe in Bakersfield than in Fresno, i.e. there is a greater increase in $PM_{2.5}$ day^{-1} over each individual event. The median increase in $PM_{2.5}$ day^{-1} event^{-1} over the last decade was 15 % greater in Bakersfield (7.9 µg m^{-3} day^{-1} event^{-1}) than Fresno (6.7 µg m^{-3} day^{-1} event^{-1}) leading to 23 % larger increases in $PM_{2.5}$ event^{-1} in Bakersfield (32.5 µg m^{-3} event^{-1}) than Fresno (25.1 µg m^{-3} event^{-1}). $PM_{2.5}$ on the first day of the event was also 20 % higher in Bakersfield (8.6 µg m^{-3} event^{-1} vs. 6.9 µg m^{-3} event^{-1}). These differences between Bakersfield and Fresno are attributed to the former's location in the southern end of the SJV, where the city is enclosed on three sides by the mountains, resulting in reduced losses to advection and mixing than in Fresno. An enhanced influence of stagnation over the NO_3^- concentration in the

Title Page

Abstract | Introduction

Conclusions | References

Tables | Figures

|◄ | ►|

◄ | ►

Back | Close

Full Screen / Esc

Printer-friendly Version

Interactive Discussion

southern SJV is reflected in the looser observed correlation (r^2) in Fig. 2 in Bakersfield (0.6) than in Fresno (0.9).

4.2 Impacts of future NO$_x$ reductions

California has committed to additional, sizable controls on NO$_x$ emissions, with de-
creases of at least 50 %, and potentially up to 75 % NO$_x$, imminent over the next decade. California has implemented a retrofit/replacement program to accelerate impacts of federal rules on diesel engines, affecting weekday NO$_x$ (Dallmann and Harley, 2010), and has both tightened standards on gasoline-powered vehicles and required one in seven new cars sold in the state be zero-emission or plug-in hybrids for model years 2017–2025 (CARB, 0.2012), affecting weekday and weekend NO$_x$.

Currently, average wintertime NO$_x$ concentrations are low enough that reductions of 50 and 75 % are calculated to decrease PNO$_3^-$ in the NRL in Bakersfield on weekends by 40 and 70 %, respectively (Fig. 7a), with similar results in Fresno and Visalia. Recall, the NO$_3$ radical production is nonlinear vs. NO$_2$ and, for a fixed O$_x$ concentration, production is described by a single curve in Fig. B1a. When O$_x$ is variable, NO$_3$ radical production is described by multiple curves, and is most sensitive to changes in O$_3$ at NO$_2$ concentrations which are at and/or greater than peak NO$_3$ radical production. At low NO$_x$ (and high NO$_x$), PNO$_3^-$ that is limited by NO$_3$ radical production is more sensitive to changes in NO$_2$. Figure 5 suggests that a direct result of decreases in NO$_2$, the chemical sensitivity of PNO$_3^-$ on NO$_2$ has been altered such that future NO$_x$ controls are poised to more effective at slowing PNO$_3^-$ in the next decade than they have over the last. We computed that NO$_x$ reductions of 50 and 75 % are large enough that changes in the average wintertime NH$_4$NO$_3$ are quantified via 2.56 : 1 line, which is the stoichiometric NO$_3^-$ response to NO$_2$, meaning the O$_3$ feedback from reduced NO$_x$ on PNO$_3^-$ is minimal. Our calculation also implies greater decreases in PNO$_3^-$ have occurred in lower-NO$_x$ rural environments than in cities since 2001 given the same relative percent NO$_x$ reductions. The highest NO$_x$ conditions in the SJV are present

in the shallowest boundary layers of December and January; we observed that during DISCOVER-AQ, NO_x concentrations were large enough that reduced weekend NO_x (21–22 January) had the effect of increasing PNO_3^- in the NRL relative to the preceding weekdays, i.e. chemistry on these days was right of peak NO_3 radical production.

For NO_x emission changes to affect daytime PNO_3^-, they must be large enough to transition photochemistry into the NO_x-limited regime, less than a few ppb in the wintertime SJV (Fig. B1b). In Bakersfield (Fig. 7b), at -50% NO_x from current levels we predict an increase in daytime NH_4NO_3 production of $2\,\mu g\,m^{-3}\,day^{-1}$ ($\sim 15\%$) but at -75% NO_x we predict a transition to low-NO_x chemistry and a net decrease in NH_4NO_3 production of $1.5\,\mu g\,m^{-3}\,day^{-1}$ (15\%). Initial enhancements in NH_4NO_3 are caused by NO_x feedbacks on the HO_x precursors, O_3 and CH_2O, which both increase in response to decreases in NO_2 (Fig. B2). In Fig. 7b, the gray line is the modeled NH_4NO_3 production day^{-1} calculated for present day conditions. The modeled points show the results of the calculations, for which the influence of NO_x decreases on PHO_x and the subsequent feedbacks on are NH_4NO_3 production are accounted. Movement of predicted NH_4NO_3 production above the gray line is due to the NO_2-PHO_x precursor feedback. In Fresno (not shown), we compute an increase of $0.5\,\mu g\,m^{-3}\,day^{-1}$ ($< 5\%$) at -50% NO_x and a decrease in NH_4NO_3 production of $\sim 3\,\mu g\,m^{-3}\,day^{-1}$ (20\%) at -75% NO_x.

Combining our derived trends in NRL and daytime PNO_3^- (Table 1), we calculate impacts of past and future NO_x controls on the frequency of wintertime 24 h $PM_{2.5}$ NAAQS exceedances. Using data from a multi-year experiment in the early 2000s (Appendix A), we found that 24 h NO_3^- was observed to be an almost constant fraction of wintertime 24 h $PM_{2.5}$ in Fresno when 24 h $PM_{2.5}$ was greater than $15\,\mu g\,m^{-3}$, and was an even larger fraction at lower loadings, typically in March. During DISCOVER-AQ, surface NO_3^- in $PM_{2.5}$ measurements in Fresno indicated 41\% (median) and 39\% (mean) of $PM_{2.5}$ was NO_3^- and 57\% (median) and 53\% (mean) was NH_4NO_3. Previous work has shown that NH_4NO_3 is a smaller portion of total $PM_{2.5}$ in Fresno than in any other location in the SJV, including Bakersfield, with rural $PM_{2.5}$ dominated by NH_4NO_3

(Zhang et al., 2010). Therefore, we applied our calculated changes in $P\mathrm{NO}_3^-$ to 50 % of $PM_{2.5}$ mass, which represents a conservative estimate.

We conclude that NO_x controls over the last decade have reduced the number of exceedances by 12–30 %, accounting for 22–60 % of the total observed change. The primary mechanism for these changes was decreased $P\mathrm{NO}_3^-$ in the NRL. In the future, a 50 % reduction in NO_x is predicted to decrease $P\mathrm{NO}_3^-$ in the NRL more efficiently and to the point where it is approximately equal to OH-initiated $P\mathrm{NO}_3^-$ on weekends. This chemical source will still be larger than daytime production on weekdays. If larger reductions of 75 % NO_x are achieved, $P\mathrm{NO}_3^-$ in the NRL will decrease sufficiently that daytime OH-initiated HNO_3 formation is predicted to become the dominant source of $\mathrm{NH}_4\mathrm{NO}_3$ on all days of the week.

Over the next decade, we predict the SJV will experience 12–21 % fewer exceedance days with a 50 % decrease in NO_x and ~ 30 % fewer exceedances with a 75 % decrease in NO_x. We have found that only $P\mathrm{NO}_3^-$ chemistry drives $\mathrm{NH}_4\mathrm{NO}_3$, not NH_3 (Fig. 2); additionally, it has been shown elsewhere that NH_3 emissions in the SJV are too great for any reasonable NH_3 control to affect $\mathrm{NH}_4\mathrm{NO}_3$ concentrations (Herner et al., 2006). While these NO_x reductions constitute a major improvement to the air quality in the SJV, and while they will also improve the SJV's severe summertime O_3 pollution (Pusede and Cohen, 2012; Pusede et al., 2014), it is evident that, in addition to inorganic nitrate, controls on the organic aerosol mass are also required to eliminate high aerosol days in the SJV. Generally speaking, regulatory policies of valley-wide inter-pollutant trading of NO_x for $PM_{2.5}$ control must be designed both with knowledge of each nonlinear $P\mathrm{NO}_3^-$ mechanism vs. NO_2. Finally, because NO_3^- is concentrated over Fresno and Bakersfield, NO_x reductions need to happen in those cities themselves, prioritizing localized interventions.

5   Conclusions

We derived trends in the wintertime production of NO_3^- (PNO_3^-) as calculated from measurements of gas-phase precursors over the last thirteen years. We used these PNO_3^- trends to explain the observed NO_3^- concentration sensitivity to NO_2, which was -0.5 and $-0.64\,\mu g\,m^{-3}\,ppb^{-1}\,NO_2$ in the San Joaquin Valley (SJV) cities of Fresno in Bakersfield, respectively. We found that reductions in NO_x have both decreased and increased NH_4NO_3 formation rates by the various chemical pathways, but that the net downward trend in NO_3^- has been driven by local changes in nighttime chemistry in residual layers decoupled from fresh surface emissions. We showed that high NH_4NO_3 abundances were a combined function of active chemical PNO_3^- and rapid atmospheric loss by deposition of gas-phase HNO_3 ($\tau_{NO_3^-} \sim 3$ daytime h); in contrast, the total aerosol mass lifetime was controlled by cold fronts that turnover valley air on average every 5 ± 1.5 days. We computed the impact of future NO_x decreases on PNO_3^- from both nighttime and daytime mechanisms, finding the sign and magnitude of the changes are dependent on oxidation pathway, oxidant precursor, NO_2 concentration, and, at night specifically, altitude. We calculated that the SJV will experience 12–21 % fewer days in exceedance of the 24 h $PM_{2.5}$ standard with a 50 % NO_x reduction and ~ 30 % fewer 24 h $PM_{2.5}$ exceedance days with a 75 % NO_x reduction. As an additional consequence of anticipated NO_x controls, daytime rather than nighttime chemistry will drive NH_4NO_3 production in the SJV in the future. The observations and calculations presented here offer improved insight into the chemistry imbedded in the wintertime NH_4NO_3 diurnal cycles and suggest such long-term measurements would inform the absolute and relative contributions by vertically stratified NO_3 chemistry vs. OH-initiated production, especially if a record that captured diurnal variability were put in place prior to the sizable NO_x reductions that are forthcoming. To conclude, the specific NO_x constraints on NH_4NO_3 chemistry we described here likely inform the effects of NO_x emission changes, both increases and decreases, on aerosol mass in polluted cities around the world.

Printer-friendly Version

Interactive Discussion

Appendix A: Measurements

A1 Long-term records

The long-term aerosol NO_3^- data are from 24 h integrated filter-based measurements of PM_{10} collected once every three to six days as part of the US EPA's Chemical Speciation Network program. The data were downloaded from the California Air Resources Board (CARB) archive (http://www.arb.ca.gov/aqmis2/aqdselect.php). We used measurements at Fresno-First Street (36.782° N, 119.773° W) and Bakersfield-5558 California Avenue (35.357° N, 119.063° W), as the two stations had mostly uninterrupted records and co-located observations of NO_2 and O_3. In Fig. 2, Bakersfield NO_3^- wintertime (November–March) medians include the years 2001–2013 with an average of 46 weekday and 18 weekend data points year^{-1}. The Fresno-First Street station was closed in 2012 and so the Fresno NO_3^- wintertime medians include 2001–2012 with an average of 36 weekday and 17 weekend data points year^{-1}.

To make these NO_3^- measurements, ambient air is sampled through a denuder and aerosol are collected on a quartz fiber filter for 24 h, midnight-to-midnight. Water-soluble ions are then quantified by ion chromatography. NH_4NO_3 is semi volatile and exists in thermal equilibrium with gas-phase HNO_3 and NH_3. Long sample collection times (24 h) and the presence of a denuder result in low biases due to loss of NO_3^- to the gas-phase (Appel et al., 1981; Shaw Jr. et al., 1982; Hering and Cass, 1999; Babich et al., 2000). This interference is well documented and observed to be large during summer months, when more than 80 % NH_4NO_3 may be lost, but is estimated to be ∼ 20 % when relative humidities are high and temperatures are cold (Appel et al., 1981; Shaw Jr. et al., 1982; Hering and Cass, 1999). If we assume ambient conditions are driving (Appel et al., 1981; Shaw Jr. et al., 1982; Hering and Cass, 1999; Babich et al., 2000), we can estimate the interference using AMS observations of NO_3^-, NH_4^+, chloride (Cl^-), and sulfate (SO_4^{2-}) and a particle into liquid sampler (PILS) of potassium (K^+) and magnesium (Mg^+) during the DISCOVER-AQ experiment to constrain

the thermodynamic model ISORROPIA II (Nenes et al., 1998; Fountoukis and Nenes, 2007). We set the total gas plus particle concentration equal to the ion data and ran the model in the forward mode to simulate the gas-aerosol partitioning after the air stream passed through a denuder, which is consistent with all of the gas being captured by the denuder and all aerosol depositing on the filter. During DISCOVER-AQ (14 January–14 February 2013) the daily average temperature and relative humidity (RH) were $8.5\,^\circ$C and 70 %, respectively. Median daytime (8 a.m.–6 p.m.) wintertime temperatures were within ~ $1\,^\circ$C and 1 % RH in Bakersfield and Fresno. When these conditions drive the interference, we predict that daily-integrated NO_3^- was biased low by 25 %, in line with other reports (Chow et al., 2005). The average wintertime (November–March) temperature and RH at the USDA Shafter Station from 2000–2013 were $10\,^\circ$C and 79 %, respectively. Under these ambient conditions, we predict measurements of the daily-integrated NO_3^- are biased low by 23 %. Evaporative loss of NO_3^- of 25 % implies the true slope is 20 % greater with respect to the measured value. The observed correlation between NO_3^- and NO_2 indicates ~ 20 % of NO_2 is oxidized to NO_3^- (Fig. 2), a 20 % NO_3^- error implies that 25 % of NO_2 is oxidized to NO_3^-.

Hourly O_3, 24 h total $PM_{2.5}$, and NO_2 data are from the CARB archive at the following sites: Fresno-First Street (2000–2011), Fresno-Garland (36.785° N, 119.773° W) (2011–2013), Visalia-North Church Street (36.333° N, 119.291° W) (2000–2013), and Bakersfield-5558 California Avenue (2000–2013). NO_2 measurements are made by chemiluminescence coupled to a heated molybdenum catalyst and have a known but poorly quantified positive interference from higher oxides of nitrogen (Winer et al., 1974; Williams et al., 1998; Dunlea et al., 2007). This interference is largest in the summertime when weakly bound higher oxides are more abundant relative to NO_x and minimal in the wintertime. These instruments sample ambient air through a filter, removing NO_3^- and likely a considerable fraction of gas-phase HNO_3 and multifunctional organic nitrates, reducing the positive artifact. NO_2 concentrations are decreasing across the valley at a rate similar to that observed from space by OMI, an instrument selective for NO_2, suggesting that relative trends in NO_2 are accurate (Russell et al., 2010).

Hourly solar radiation, temperature, and RH data are from the California Irrigation Management Information System archive (http://wwwcimis.water.ca.gov/Default.aspx) at the Shafter US Department of Agriculture (USDA) station (35.530° N, 119.280° W). Sunrise and sunset times in Bakersfield (35.357° N, 119.063° W) were downloaded from the United States Naval Observatory Naval Oceanography Portal (http://aa.usno.navy.mil/data/docs/RS_OneYear.php).

Nitrate ion observations with 10 min time resolution were available during select time periods and were used to determine the wintertime variability in the fraction of $PM_{2.5}$ that was NO_3^-. There data were collected in Fresno in 2000–2001 and 2003–2005 (Watson et al., 2000) as part of the EPA PM Supersites program (http://www.epa.gov/ttnamti1/supersites.html). These measurements were made by flash volatizing NH_4NO_3, reducing HNO_3 across a heated catalyst to nitric oxide (NO), and detecting NO by chemiluminescence (Stolzenburg et al., 2003; Chow et al., 2008). It was reported that 24 h averages of these high-time resolution observations were well correlated with, but 20–40 % lower than, 24 h $PM_{2.5}$ filter samples (annual averages). This effect has been attributed to incomplete volatization and/or incomplete catalytic conversion of NO_3^- to NO. Two identical instruments at the Fresno supersite yielded data that were also well correlated but different by 10–55 % in the annual average (Chow et al., 2008). We treat these observations as uncalibrated but internally consistent over time.

A2 DISCOVER-AQ observations

The DISCOVER-AQ experiment synchronized multiple ground sites and aircraft sampling of in situ and column measurements, producing a dataset resolved in space, both horizontally and vertically, and in time. The DISCOVER-AQ sampling strategy was built on repeated sampling across urban-rural (horizontal) and vertical gradients and on connecting observations made from balloons, onboard aircraft, and from space to monitoring sites at the surface. The NASA P-3B aircraft flew 2–3 identical circuits day^{-1}, alternating low altitude (150 m a.g.l.), along the valley's western edge, medium-low

(300 m a.g.l.) and high altitude flight passes (2.6 km a.g.l.). Circuits included missed approaches at all cities and rural waypoints when visibility permitted. Missed approaches allowed the P-3B to reach altitudes as low as 20–40 m a.g.l.) and were conducted over airstrips. Landing strips were often rural and little trafficked but may have experienced airport-related NO$_x$ enhancements in the cities of Fresno and Bakersfield.

The comprehensive suite of DISCOVER-AQ data is available to the public at: https://www-air.larc.nasa.gov/cgi-bin/ArcView/discover-aq.ca-2013. Table A1 lists the measurement accuracy, analytical technique, platform and location, and associated references of species key to this analysis.

The NO$_3^-{}_{(g+p)}$ measurements were made by thermal dissociation laser induced fluorescence (TD-LIF). The TD-LIF operating principle is as follows: NO$_2$ is detected by laser-induced fluorescence (LIF) (Thornton et al., 1999). A tunable dye laser is pumped by a Q-switched, frequency doubled Nd^{3+}:YAG laser. The narrow band dye laser is etalon-tuned to a specific 585 nm rovibronic feature of NO$_2$, alternating between this feature and the weaker continuum absorption. The resulting red-shifted photons are imaged onto a photomultiplier tube and collected using time-gated counting. The LIF technique is spectroscopically specific and accurate (±5 %). The system was calibrated in flight every ∼ 30 min with an NO$_2$ reference standard added at the inlet. The higher oxides of nitrogen, peroxy nitrates (RO$_2$NO$_2$), alkyl nitrates (RONO$_2$), and HNO$_3$ are measured by thermal dissociation (TD) coupled to LIF (Day et al., 2002). Dissociation of thermally labile species into NO$_2$ and a companion radical occurs at characteristic temperatures due to differing N–O bond strengths. Ambient air is pulled through heated quartz tube ovens followed by PFA sampling lines before reaching the NO$_2$ detection cell. An unheated channel detects only NO$_2$, a second channel (180 °C) measures NO$_2$ + RO$_2$NO$_2$, a third channel (400 °C) measures NO$_2$ + RO$_2$NO$_2$ + RONO$_{2(g+p)}$, and a fourth (600 °C) measures NO$_2$ + RO$_2$NO$_2$ + RONO$_{2(g+p)}$ + NO$_3^-{}_{(g+p)}$. Mixing ratios of each species are determined as the difference between adjacent channels, i.e. NO$_3^-{}_{(g+p)}$ equals the 600 °C channel minus the signal in the 400 °C channel.

Particles smaller than 2.5 µm are thought to be efficiently transmitted through the inlet to the TD-LIF system. Measurements of $NO_{3\,(g+p)}^-$ typically agreed with an onboard PILS system (4 min time resolution) with an ~ 3 µm aerosol size cutoff and detecting only particle-phase NO_3^-, indicating the two instruments sampled aerosol of similar sizes, that the bulk of $NO_{3\,(g+p)}^-$ was in the aerosol phase, and that inlet losses of $NO_{3\,(g+p)}^-$ were minimal. Additional details on the TD-LIF aircraft inlet configuration are found in Perring et al. (2009) and Wooldridge et al. (2010).

A sample of TD-LIF data collected during a morning flight segment is shown in Fig. A1, where at least two residual layers are visible; however, due to a combination of an extremely shallow NBL and the $NO_{3\,(g+p)}^-$ sampling cycle, it is unclear whether the surface mixed layer was indeed captured. The indication of the surface air would have been low to zero O_3 concentrations with concurrent $NO_{3\,(g+p)}^-$ measurements.

A3 Data and filtering for boundary layer sampling

Regarding measurements made onboard the P-3B aircraft, on some occasions, the height of the daytime boundary layer was observed near the altitude of the P-3B's low-level flight legs, requiring analysis to distinguish between free troposphere and boundary layer air. Within boundary layer sampling was confirmed using 1 s^{-1} measurements of NO and RH recorded by the aircraft PDS, according to steep discontinuities in both tracers, being high in the boundary layer and low aloft. In some cases, $H_2O_{(v)}$ measured by diode laser hygrometer (DLH) and O_3 were also considered.

For our derivation of $\tau_{NO_3^-}$, to estimate the boundary layer depth we referred to a micro-pulse lidar (MPL) located in the town of Porterville during DISCOVER-AQ. The MPL was supplemented with a wide-field receiver system that allowed for improved near-range signal recovery of the 527 nm attenuated backscatter profiles that were recorded at 30 m vertical and 1 min time resolutions. For daytime mixed-layer conditions driven by convection, the aerosol gradient falls off and stable molecular scatter signal above the lowest mixed aerosol layer signal represents the boundary layer height. Ac-

Printer-friendly Version

Interactive Discussion

cording to this aerosol gradient, boundary layer heights were observed to range from 300 to 700 m during DISCOVER-AQ.

Appendix B: Calculating PNO_3^-

The chemistry producing NO_3 radical at night and HNO_3 in the daytime vs. NO_2 is shown in Fig. B1. In Fig. B1a, the production of NO_3 radical ($\mu g\,m^{-3}\,h^{-1}$) is calculated at four initial O_x ($O_x \equiv NO_2 + O_3$) conditions: 50 ppb O_x (black), 40 ppb O_x (purple), 30 ppb O_x (violet), and 20 ppb O_x (gray). In Fig. B1b, the production of HNO_3 is shown for two PHO_x conditions: 0.3 ppt s^{-1} PHO_x (orange) and 0.15 ppt s^{-1} PHO_x (golden). The same equations that produced Fig. B1 were used to compute PNO_3^-.

B1 NO_3-initiated PNO_3^- in the nocturnal residual layer (NRL)

Our time-dependent box model of NO_3 radical production was run separately for each day over the time period 2000–2013. The model was initialized with hourly O_3 measurements at the surface using the maximum concentration 1–3 h before sunset and the median daytime (10 a.m.–3 p.m. LT) NO_x. The time window was determined based on the timing of steep afternoon O_3 titration at the surface. Both O_3 and NO_x were treated as well mixed in the daytime boundary layer, a good assumption in the afternoon. $k_{NO_2+O_3}$ was calculated based on the mean surface temperature at 6–8 p.m. LT. NO_3 radical production was integrated from sunset to 1 h prior to sunrise. Insignificant differences were observed using the mean O_3 over this time window and daily maximum O_3.

Reaction fates of NO_3 radicals calculated by the time-dependent box model described above were determined according to the proportional NO_3 reactivity contributions observed during DISCOVER-AQ. The reaction pathways of NO_3 are as follows

(BR1–BR3):

$$NO_3 + NO_2 \rightarrow N_2O_5 \tag{BR1}$$
$$NO_3 + \text{alkene} \rightarrow RONO_2 \tag{BR2}$$
$$NO_3 + \text{aldehyde or alcohol or dimethyl sulfide} \rightarrow HNO_3 + \text{products} \tag{BR3}$$

Each of the three pathways results in a different number of NO_3^- produced per NO_3 radical. NO_3 reactivities in Fresno and Bakersfield were computed using the DISCOVER-AQ dataset with daytime (10 a.m.–5 p.m. LT) surface observations of NO_2, organic compounds (whole air canister sampling), and dimethyl sulfide (DMS) (whole air canister sampling). CH_2O measurements from onboard the P3-B were included in the speciated reactivity by R5. In both Fresno and Bakersfield, the reaction of NO_2 with NO_3 represented $\sim 85\%$ of total NO_3 reactivity, with negligible weekday-weekend differences. The median NO_3 reactivity values used in the model were: $0.03\,s^{-1}$ for addition to double bonds, yielding $0\,HNO_3$; $< 0.001\,s^{-1}$ for hydrogen abstraction, yielding $1\,HNO_3$; and $0.2\,s^{-1}$ for reaction with NO_2, which after heterogeneous conversion of N_2O_5 yields $2\,HNO_3$. This gives $1.7\,NO_3^-$ produced per NO_3, on average. The integrated $P\text{NO}_3^-$ was taken as the NO_3 radical production scaled by the NO_3 reactivity to NO_2, which assumed reactions with alkenes and DMS were instantaneous. This result is similar to that of the wintertime NACHTT experiment at comparable relative NO_2 concentrations (Wagner et al., 2013), during which, NO_3 and N_2O_5 were measured, the kinetics of N_2O_5 explicitly included in the calculation of $P\text{NO}_3^-$, and $1.6\,HNO_3$ per NO_3 radical produced was inferred.

B2 NO_3-initiated $P\text{NO}_3^-$ in the nocturnal boundary layer (NBL)

The production of NO_3 radical was directly computed from surface measurements of hourly O_3, NO_2, NO, and temperature each day from 2000–2013. NO_3 production was integrated between sunset and 1 h prior to sunrise and scaled by 1.7. There were times that under conditions of very high NO that nighttime O_3 was observed to be positive

and constant at nonphysical values of 1–10 ppb for multiple hours. This offset was interpreted as a measurement artifact as excess NO titrates O_3 completely. To account for this, when NO_x was greater than five times the reported O_3, O_3 was set equal to zero prior to computing NO_3 production.

B3   OH-initiated PNO_3^-

The integrated daily production of HNO_3 was calculated for each day from 2000–2013 separately for each of the three HO_x sources: $O(^1D) + H_2O$, HONO photolysis, and CH_2O photolysis (Eq. B1). PNO_3^- vs. NO_2 attributed to each HO_x source is plotted in Fig. B2. OH was modeled with an analytical model constrained to DISCOVER-AQ observations, built on the assumption that oxidizing radicals were in steady state (Eq. B2) and that RO_2 and HO_2 production are approximately equal, as are RO_2 production and loss, giving Eq. (B2) for both RO_2 and HO_2 (Eq. B3) (Murphy et al., 2007). The symbol α is the $RONO_2$ branching ratio. RO_2NO_2 are considered to be in thermal equilibrium with NO_2 and peroxy radicals, and therefore not to contribute to net radical formation. Calculated wintertime OH values were $\sim 10^6$ molecules cm^{-3} at noontime and exhibited reasonable nonlinear NO_2 dependence throughout the day. Observational inputs to the model were NO and NO_2, the total organic reactivity to OH (VOCR), PHO_x, α, and temperature. VOCR was computed as equal to $\sum_i k_{OH+VOC_i}[VOC_i]$ using whole air samples of speciated organic molecules collected at the ground during DISCOVER-AQ and CH_2O data from onboard the P-3B, as VOCR equal to $\sum_i k_{OH+VOC_i}[VOC_i]$. The daytime average was $\sim 4 \, s^{-1}$, consistent with a recent analysis of the temperature dependence of total VOCR in Bakersfield (Pusede et al., 2014), giving confidence that the majority of the reactivity was accounted for. The α is set equal to 2 %. Equations

(B2) and (B3) are combined to solve for OH.

$$PHO_x = 2j_{O_3 \rightarrow O^1D}[O_3]\frac{k[H_2O]}{k[H_2O] + k[N_2 + O_2]} + 2j_{CH_2O}[CH_2O] + j_{HONO}[HONO] \quad (B1)$$

$$PHO_x = LHO_x = 2k_{HO_2+HO_2}[HO_2]^2 + 2k_{HO_2+RO_2}[HO_2][RO_2] + 2k_{RO_2+RO_2}[RO_2]^2$$
$$+ k_{NO_2+OH}[NO_2][OH] + \alpha k_{NO+RO_2}[NO][RO_2] \quad (B2)$$

$$5 \quad [RO_2] \sim [HO_2] = \frac{VOCR[OH]}{(1-\alpha)k_{NO+RO_2}[NO]} \quad (B3)$$

Noontime j_{O_3}, j_{HONO}, and j_{CH_2O} were computed with the TUV calculator, http://cprm.acd.ucar.edu/Models/TUV/Interactive_TUV (Madronich, 1987), on a clear-sky day (20 January 2013), scaled by the ratio of the TUV j_{NO_2} and a measurement of j_{NO_2} made onboard the P-3B, and combined with the diurnally varying long-term record of solar radiation.

10   The trend in $O(^1D) + H_2O$ was calculated from the observational record of O_3, RH, and solar radiation.

No multi-year measurements of HONO have been reported in US cities. HONO is formed at night by a mechanism functionally equivalent to the conversion of two NO_2 to one gas-phase HONO and one ground-surface adsorbed HNO_3 molecule (Finlayson-
15   Pitts et al., 2003). We computed HONO as equal to 4 % the nighttime (10 p.m.–6 a.m. LT) mean NO_2 (Stutz et al., 2004), yielding one HONO data point for each day. This HONO initialized a calculation wherein photolytic loss was computed, giving HONO concentrations at 1 h time resolution. We have not accounted for daytime forma-
20   tion; however, in total, daytime source(s) are weekday-weekend independent (Pusede et al., 2015).

The inter-annual trend in CH_2O is also unconstrained with observations. In the winter, CH_2O is not monitored at the surface and cannot be quantified from space due to low column concentrations and shallow daytime boundary layers. CH_2O is a primary or-
25   ganic emission from agricultural activities associated with animal feeds (Howard et al.,

NO_x control over ammonium nitrate

S. E. Pusede et al.

Title Page

Abstract | Introduction

Conclusions | References

Tables | Figures

|◄ | ►|

◄ | ►

Back | Close

Full Screen / Esc

Printer-friendly Version

Interactive Discussion

2010), dairy cows (Shaw et al., 2007), and combustion. State inventories offer little in-sight into CH_2O trends, as it is unknown whether a priori accounts are complete. CH_2O is also the oxidation product of most organic molecules in the atmosphere. We calcu-lated the CH_2O concentration using a 0-D chemical model constrained to the complete 1 min DISCOVER-AQ dataset. All 95 organic molecules measured by whole air sam-pling at the ground level at the Fresno site were included after scaling by a fit to aircraft carbon monoxide. Within the boundary layer, modeled CH_2O typically captured 75 % of the CH_2O measured on the P-3, with the discrepancy most likely due to the local pri-mary CH_2O emissions. We ran the model under four NO_x reduction scenarios, -75% NO_x, -50% NO_x, $+50\%$ NO_x, and $+75\%$ NO_x assuming the portion of CH_2O not captured by our model remained constant. At 50 % higher NO_x, i.e. at the start of the record, secondary CH_2O was $\sim 10\%$ lower on weekdays and $\sim 5\%$ lower on weekends than in the base model (2013 conditions). At -50 and -75% NO_x, in the next decade, secondary CH_2O is predicted to increase by 15–25 % from 2013 weekend NO_x levels, as reductions in NO_x increase OH.

The integrated wintertime PNO_3^- for each of the three HO_x sources is shown in Fig. B2, along with the projected response of PNO_3^- to changes in NO_x of -50 and -75% from weekend concentrations. PNO_3^- attributed to $O(^1D) + H_2O$ is 1–$2\,\mu g\,m^{-3}\,day^{-1}$ (2000–2013) and has increased by $\sim 0.1\,\mu g\,m^{-3}\,ppb^{-1}\,NO_2$ in all three SJV cities. It is an order of magnitude smaller than PNO_3^- in the NRL in the wintertime average. PNO_3^- attributed to HONO has decreased with reduced NO_2, i.e. the trend has the correct sign. The resulting decrease in PNO_3^- caused by decreasing HONO is 25 and 20 % in Fresno and Bakersfield, respectively, with 2–$5\,\mu g\,m^{-3}\,day^{-1}$ over the en-tire NO_2 range, despite a reduction in daytime NO_2 of 40–50 % (on weekdays). We find that CH_2O, observed to be 2.3 ± 1.1 ppb (1σ variability) in Fresno and 2.0 ± 0.9 ppb in Bakersfield, has been the largest contributor to photochemical production of NH_4NO_3 at $\sim 6\,\mu g\,m^{-3}\,day^{-1}\,NO_3^-$.

Full Screen / Esc

Printer-friendly Version

Interactive Discussion

Appendix C

The timing of decoupling between the NBL and the NRL(s) has implications for our derivation of $\tau_{NO_3^-}$. Observed daily $\frac{\partial NO_3^-}{\partial t}$ are consistent with the majority of NO_3^- lost via deposition of $HNO_{3(g)}$ from most of the daytime boundary layer. If loss occurred from only the lowest 50 m of the daytime boundary layer, then the observationally derived $HNO_{3(g)}$ v_d would be only $0.4\,cm\,s^{-1}$, below direct measurements (e.g., Huebert and Robert, 1985; Meyers et al., 1989; Sievering et al., 2001; Volpe Horii et al., 2005; Farmer et al., 2006). Gaseous HNO_3 that does not deposit will repartition to the aerosol phase when temperatures fall and RH rises in the evening. Assuming an NBL height of 50–100 m, then a nighttime rise (black data in Fig. 6) of 10–5 fold is expected. An NO_3^- concentration of $10\,\mu g\,m^{-3}$ shifted to the gas-phase would increase by 100–$50\,\mu g\,m^{-3}$ at nightfall. By contrast, typical nighttime increases were 0–$15\,\mu g\,m^{-3}$.

In Fig. C1 we show low altitude (20–350 m a.g.l.) observations from the P-3B colored by $NO_{3\,(g+p)}^-$ concentration over the city of Visalia on five flight days as evidence that afternoon decreases are net $HNO_3 + NO_3^-$ loss and not a shift in partitioning between the two species. In each panel the left-hand flight track was at midday (12–1 p.m. LT) and the right-hand track, shifted in space by 0.02° longitude for visual clarity, was in afternoon (3–4 p.m. LT). On each of the 5 flights, ∼ two-fold higher concentrations of $NO_{3\,(g+p)}^-$ were observed at midday compared to a few hours later. Additionally, the reduction in $NO_{3\,(g+p)}^-$ is apparent at the higher altitudes, shown in the top and bottom third of each panel, suggesting the loss in NO_3^- measured by AMS at the surface in Fresno does extend up to at least 300–350 m a.g.l.

for the j_{NO_2} and RH (PDS) data, Glenn Diskin for the $H_2O_{(v)}$ (DLH) data, and Donald Blake for the speciated organic compound data. The DISCOVER-AQ experiment would not have been possible without the work of the pilots, crew, and engineers of the NASA P-3B.

References

Appel, B. R., Tokiwa, Y., and Haik, M.: Sampling of nitrates in ambient air, Atmos. Environ., 15, 283–289, doi:10.1016/0004-6981(81)90029-9, 1981.

Babich, P., Davey, M., Allen, G., and Koutrakis, P.: Method comparisons for particulate nitrate, elemental carbon, and $PM_{2.5}$ mass in seven US cities, J. Air Waste Manage., 50, 1095–1105, doi:10.1080/10473289.2000.10464152, 2000.

Bertram, T. H. and Thornton, J. A.: Toward a general parameterization of N_2O_5 reactivity on aqueous particles: the competing effects of particle liquid water, nitrate and chloride, Atmos. Chem. Phys., 9, 8351–8363, doi:10.5194/acp-9-8351-2009, 2009.

Bertram, T. H., Thornton, J. A., Riedel, T. P., Middlebrook, A. M., Bahreini, R., Bates, T. S., Quinn, P. K., and Coffman, D. J.: Direct observations of N_2O_5 reactivity on ambient aerosol particles, Geophys. Res. Lett., 36, L19803, doi:10.1029/2009GL040248, 2009.

Bianco, L., Djalalova, I. V., King, C. W., and Wilczak, J. M.: Diurnal evolution and annual variability of boundary-layer height and its correlation to other meteorological variables in California's Central Valley, Bound.-Lay. Meteorol., 140, 491–511, doi:10.1007/s10546-011-9622-4, 2011.

Brown, S. G., Hyslop, N. P., Roberts, P. T., McCarthy, M. C., and Lurmann, F. W.: Wintertime vertical variations in particulate matter (PM) and precursor concentrations in the San Joaquin Valley during the California Regional Coarse PM/Fine PM Air Quality Study, J. Air Waste Manage., 56, 1267–1277, doi:10.1080/10473289.2006.10464583, 2006.

Brown, S. S. and Stutz, J.: Nighttime radical observations and chemistry, Chem. Soc. Rev., 41, 6405–6447, doi:10.1039/C2CS35181A, 2012.

Brown, S. S., Dubé, W. P., Osthoff, H. D., Wolfe, D. E., Angevine, W. M., and Ravishankara, A. R.: High resolution vertical distributions of NO_3 and N_2O_5 through the nocturnal boundary layer, Atmos. Chem. Phys., 7, 139–149, doi:10.5194/acp-7-139-2007, 2007.

Brown, S. S., Dube, W. P., Fuchs, H., Ryerson, T. B., Wollny, A. G., Brock, C. A., Bahreini, R., Middlebrook, A. M., Neuman, J. A., Atlas, E., Roberts, J. M., Osthoff, H. D., Trainer, M.,

Title Page

Abstract | Introduction

Conclusions | References

Tables | Figures

◄ | ►

◄ | ►

Back | Close

Full Screen / Esc

Printer-friendly Version

Interactive Discussion

Fehsenfeld, F. C., and Ravishankara, A. R.: Reactive uptake coefficients for N_2O_5 determined from aircraft measurements during the Second Texas Air Quality Study: comparison to current model parameterizations, J. Geophys. Res.-Atmos., 114, D00F10, doi:10.1029/2008jd011679, 2009.

5 Chen, L. W. A., Watson, J. G., Chow, J. C., and Magliano, K. L.: Quantifying $PM_{2.5}$ source contributions for the San Joaquin Valley with multivariate receptor models, Environ. Sci. Technol., 41, 2818–2826, doi:10.1021/es0525105, 2007.

Chow, J., Watson, J., Lowenthal, D., Park, K., Doraiswamy, P., Bowers, K., and Bode, R.: Continuous and filter-based measurements of $PM_{2.5}$ nitrate and sulfate at the Fresno Supersite,
10 Environ. Monit. Assess., 144, 179–189, doi:10.1007/s10661-007-9987-5, 2008.

Chow, J. C., Watson, J. G., Lowenthal, D. H., and Magliano, K. L.: Loss of $PM_{2.5}$ nitrate from filter samples in Central California, J. Air Waste Manage., 55, 1158–1168, doi:10.1080/10473289.2005.10464704, 2005.

Chow, J. C., Chen, L. W. A., Watson, J. G., Lowenthal, D. H., Magliano, K. A., Turkiewicz, K.,
15 and Lehrman, D. E.: $PM_{2.5}$ chemical composition and spatiotemporal variability during the California Regional $PM_{10}/PM_{2.5}$ Air Quality Study (CRPAQS), J. Geophys. Res.-Atmos., 111, D10S04, doi:10.1029/2005jd006457, 2006a.

Chow, J. C., Watson, J. G., Lowenthal, D. H., Chen, L. W. A., Tropp, R. J., Park, K., and Magliano, K. A.: $PM_{2.5}$ and PM_{10} mass measurements in California's San Joaquin Valley,
20 Aerosol Sci. Tech., 40, 796–810, doi:10.1080/02786820600623711, 2006b.

Clarisse, L., Shephard, M. W., Dentener, F., Hurtmans, D., Cady-Pereira, K., Karagulian, F., Van Damme, M., Clerbaux, C., and Coheur, P.-F.: Satellite monitoring of ammonia: a case study of the San Joaquin Valley, J. Geophys. Res.-Atmos., 115, D13302, doi:10.1029/2009jd013291, 2010.

25 Dallmann, T. R. and Harley, R. A.: Evaluation of mobile source emission trends in the United States, J. Geophys. Res.-Atmos., 115, D14305, doi:10.1029/2010jd013862, 2010.

Dallmann, T. R., DeMartini, S. J., Kirchstetter, T. W., Herndon, S. C., Onasch, T. B., Wood, E. C., and Harley, R. A.: On-road measurement of gas and particle phase pollutant emission factors for individual heavy-duty diesel trucks, Environ. Sci. Technol., 46, 8511–8518,
30 doi:10.1021/es301936c, 2012.

Day, D. A., Wooldridge, P. J., Dillon, M. B., Thornton, J. A., and Cohen, R. C.: A thermal dissociation laser-induced fluorescence instrument for in situ detection of NO_2, peroxy ni-

Title Page

Abstract	Introduction
Conclusions	References
Tables	Figures

◀◀   ▶▶

◀   ▶

Back   Close

Full Screen / Esc

Printer-friendly Version

Interactive Discussion

trates, alkyl nitrates, and HNO$_3$, J. Geophys. Rese.-Atmos., 107, ACH 4-1–ACH 4-14, doi:10.1029/2001JD000779, 2002.

Dentener, F. J. and Crutzen, P. J.: Reaction of N$_2$O$_5$ on tropospheric aerosols – impact on the global distributions of NO$_x$, O$_3$, and OH, J. Geophys. Res.-Atmos., 98, 7149–7163, doi:10.1029/92jd02979, 1993.

Drewnick, F., Hings, S. S., DeCarlo, P., Jayne, J. T., Gonin, M., Fuhrer, K., Weimer, S., Jimenez, J. L., Demerjian, K. L., Borrmann, S., and Worsnop, D. R.: A new Time-of-Flight Aerosol Mass Spectrometer (TOF-AMS) – instrument description and first field deployment, Aerosol Sci. Tech., 39, 637–658, doi:10.1080/02786820500182040, 2005.

Dunlea, E. J., Herndon, S. C., Nelson, D. D., Volkamer, R. M., San Martini, F., Sheehy, P. M., Zahniser, M. S., Shorter, J. H., Wormhoudt, J. C., Lamb, B. K., Allwine, E. J., Gaffney, J. S., Marley, N. A., Grutter, M., Marquez, C., Blanco, S., Cardenas, B., Retama, A., Ramos Villegas, C. R., Kolb, C. E., Molina, L. T., and Molina, M. J.: Evaluation of nitrogen dioxide chemiluminescence monitors in a polluted urban environment, Atmos. Chem. Phys., 7, 2691–2704, doi:10.5194/acp-7-2691-2007, 2007.

Farmer, D. K., Wooldridge, P. J., and Cohen, R. C.: Application of thermal-dissociation laser induced fluorescence (TD-LIF) to measurement of HNO$_3$, $\sum$ alkyl nitrates, $\sum$ peroxy nitrates, and NO$_2$ fluxes using eddy covariance, Atmos. Chem. Phys., 6, 3471–3486, doi:10.5194/acp-6-3471-2006, 2006.

Finlayson-Pitts, B. J., Wingen, L. M., Sumner, A. L., Syomin, D., and Ramazan, K. A.: The heterogeneous hydrolysis of NO$_2$ in laboratory systems and in outdoor and indoor atmospheres: an integrated mechanism, Phys. Chem. Chem. Phys., 5, 223–242, doi:10.1039/b208564j, 2003.

Flechard, C. R., Spirig, C., Neftel, A., and Ammann, C.: The annual ammonia budget of fertilised cut grassland – Part 2: Seasonal variations and compensation point modeling, Biogeosciences, 7, 537–556, doi:10.5194/bg-7-537-2010, 2010.

Fountoukis, C. and Nenes, A.: ISORROPIA II: a computationally efficient thermodynamic equilibrium model for K$^+$–Ca^{2+}–Mg^{2+}–NH$_4^+$–Na$^+$–SO$_4^{2-}$–NO$_3^-$–Cl$^-$–H$_2$O aerosols, Atmos. Chem. Phys., 7, 4639–4659, doi:10.5194/acp-7-4639-2007, 2007.

Ge, X., Setyan, A., Sun, Y., and Zhang, Q.: Primary and secondary organic aerosols in Fresno, California during wintertime: results from high resolution aerosol mass spectrometry, J. Geophys. Res.-Atmos., 117, D19301, doi:10.1029/2012JD018026, 2012.

NO$_x$ control over ammonium nitrate

S. E. Pusede et al.

Gilliland, A. B., Appel, K. W., Pinder, R. W., and Dennis, R. L.: Seasonal NH_3 emissions for the continental united states: inverse model estimation and evaluation, Atmos. Environ., 40, 4986–4998, doi:10.1016/j.atmosenv.2005.12.066, 2006.

Goebes, M. D., Strader, R., and Davidson, C.: An ammonia emission inventory for fertilizer application in the United States, Atmos. Environ., 37, 2539–2550, doi:10.1016/s1352-2310(03)00129-8, 2003.

Heald, C. L., Collett Jr., J. L., Lee, T., Benedict, K. B., Schwandner, F. M., Li, Y., Clarisse, L., Hurtmans, D. R., Van Damme, M., Clerbaux, C., Coheur, P.-F., Philip, S., Martin, R. V., and Pye, H. O. T.: Atmospheric ammonia and particulate inorganic nitrogen over the United States, Atmos. Chem. Phys., 12, 10295–10312, doi:10.5194/acp-12-10295-2012, 2012.

Hering, S. and Cass, G.: The magnitude of bias in the measurement of $PM_{2.5}$ arising from volatilization of particulate nitrate from teflon filters, J. Air Waste Manage., 49, 725–733, doi:10.1080/10473289.1999.10463843, 1999.

Herner, J. D., Ying, Q., Aw, J., Gao, O., Chang, D. P. Y., and Kleeman, M. J.: Dominant mechanisms that shape the airborne particle size and composition distribution in Central California, Aerosol Sci. Tech., 40, 827–844, doi:10.1080/02786820600728668, 2006.

Holets, S. and Swanson, R. N.: High-inversion fog episodes in Central California, J. Appl. Meteorol., 20, 890–899, doi:10.1175/1520-0450(1981)020<0890:HIFEIC>2.0.CO;2, 1981.

Howard, C. J., Kumar, A., Malkina, I., Mitloehner, F., Green, P. G., Flocchini, R. G., and Kleeman, M. J.: Reactive organic gas emissions from livestock feed contribute significantly to ozone production in Central California, Environ. Sci. Technol., 44, 2309–2314, doi:10.1021/es902864u, 2010.

Huebert, B. J. and Robert, C. H.: The dry deposition of nitric acid to grass, J. Geophys. Res.-Atmos., 90, 2085–2090, doi:10.1029/JD090iD01p02085, 1985.

Jacob, D. J., Waldman, J. M., Munger, J. W., and Hoffmann, M. R.: A field investigation of physical and chemical mechanisms affecting pollutant concentrations in fog droplets, Tellus, 36, 272–285, 1984.

Jacob, D. J., Munger, J. W., Waldman, J. M., and Hoffmann, M. R.: The H_2SO_4-HNO_3-NH_3 system at high humidities and in fogs. 1. Spatial and temporal patterns in the San Joaquin Valley of California, J. Geophys. Res.-Atmos., 91, 1073–1088, doi:10.1029/JD091iD01p01073, 1986a.

Title Page

Abstract | Introduction

Conclusions | References

Tables | Figures

|◄ | ►|

◄ | ►

Back | Close

Full Screen / Esc

Printer-friendly Version

Interactive Discussion

Jacob, D. J., Waldman, J. M., Munger, J. W., and Hoffmann, M. R.: The H_2SO_4-HNO_3-NH_3 system at high humidities and in fogs. 2. Comparison of field data with thermodynamic calculations, J. Geophys. Res.-Atmos., 91, 1089–1096, doi:10.1029/JD091iD01p01089, 1986b.

Kelly, J. T., Baker, K. R., Nowak, J. B., Murphy, J. G., Markovic, M. Z., VandenBoer, T. C., Ellis, R. A., Neuman, J. A., Weber, R. J., Roberts, J. M., Veres, P. R., de Gouw, J. A., Beaver, M. R., Newman, S., and Misenis, C.: Fine-scale simulation of ammonium and nitrate over the South Coast Air Basin and San Joaquin Valley of California during CalNex-2010, J. Geophys. Res.-Atmos., 119, 3600–3614, doi:10.1002/2013jd021290, 2014.

Macintyre, H. L. and Evans, M. J.: Sensitivity of a global model to the uptake of N_2O_5 by tropospheric aerosol, Atmos. Chem. Phys., 10, 7409–7414, doi:10.5194/acp-10-7409-2010, 2010.

Madronich, S.: Photodissociation in the atmosphere. 1. Actinic flux and the effects of ground reflections and clouds, J. Geophys. Res.-Atmos., 92, 9740–9752, doi:10.1029/JD092iD08p09740, 1987.

McDonald, B. C., Dallmann, T. R., Martin, E. W., and Harley, R. A.: Long-term trends in nitrogen oxide emissions from motor vehicles at national, state, and air basin scales, J. Geophys. Res.-Atmos., 117, D00V18, doi:10.1029/2012jd018304, 2012.

Meyers, T. P., Huebert, B. J., and Hicks, B. B.: HNO_3 deposition to a deciduous forest, Bound.-Lay. Meteorol., 49, 395–410, doi:10.1007/BF00123651, 1989.

Munger, J. W., Jacob, D. J., Waldman, J. M., and Hoffmann, M. R.: Fogwater chemistry in an urban atmosphere, J. Geophys. Res.-Oceans Atmos., 88, 5109–5121, doi:10.1029/JC088iC09p05109, 1983.

Murphy, J. G., Day, D. A., Cleary, P. A., Wooldridge, P. J., Millet, D. B., Goldstein, A. H., and Cohen, R. C.: The weekend effect within and downwind of Sacramento – Part 1: Observations of ozone, nitrogen oxides, and VOC reactivity, Atmos. Chem. Phys., 7, 5327–5339, doi:10.5194/acp-7-5327-2007, 2007.

Nenes, A., Pandis, S., and Pilinis, C.: ISORROPIA: a new thermodynamic equilibrium model for multiphase multicomponent inorganic aerosols, Aquat. Geochem., 4, 123–152, doi:10.1023/A:1009604003981, 1998.

Pandis, S. N. and Seinfeld, J. H.: On the interaction between equilibration processes and wet or dry deposition, Atmos. Environ., 24, 2313–2327, doi:10.1016/0960-1686(90)90325-H, 1990.

Perring, A. E., Bertram, T. H., Wooldridge, P. J., Fried, A., Heikes, B. G., Dibb, J., Crounse, J. D., Wennberg, P. O., Blake, N. J., Blake, D. R., Brune, W. H., Singh, H. B., and Cohen, R. C.:

Airborne observations of total RONO$_2$: new constraints on the yield and lifetime of isoprene nitrates, Atmos. Chem. Phys., 9, 1451–1463, doi:10.5194/acp-9-1451-2009, 2009.

Pleim, J. E., Bash, J. O., Walker, J. T., and Cooter, E. J.: Development and evaluation of an ammonia bidirectional flux parameterization for air quality models, J. Geophys. Res.-Atmos., 118, 3794–3806, doi:10.1002/jgrd.50262, 2013.

Pusede, S. E. and Cohen, R. C.: On the observed response of ozone to NO$_x$ and VOC reactivity reductions in San Joaquin Valley California 1995–present, Atmos. Chem. Phys., 12, 8323–8339, doi:10.5194/acp-12-8323-2012, 2012.

Pusede, S. E., Gentner, D. R., Wooldridge, P. J., Browne, E. C., Rollins, A. W., Min, K.-E., Russell, A. R., Thomas, J., Zhang, L., Brune, W. H., Henry, S. B., DiGangi, J. P., Keutsch, F. N., Harrold, S. A., Thornton, J. A., Beaver, M. R., St. Clair, J. M., Wennberg, P. O., Sanders, J., Ren, X., VandenBoer, T. C., Markovic, M. Z., Guha, A., Weber, R., Goldstein, A. H., and Cohen, R. C.: On the temperature dependence of organic reactivity, nitrogen oxides, ozone production, and the impact of emission controls in San Joaquin Valley, California, Atmos. Chem. Phys., 14, 3373–3395, doi:10.5194/acp-14-3373-2014, 2014.

Pusede, S. E., VandenBoer, T. C., Murphy, J. G., Markovic, M. Z., Young, C. J., Veres, P. R., Roberts, J. M., Washenfelder, R. A., Brown, S. S., Ren, X., Tsai, C., Stutz, J., Brune, W. H., Browne, E. C., Wooldridge, P. J., Graham, A. R., Weber, R., Goldstein, A. H., Dusanter, S., Griffith, S. M., Stevens, P. S., Lefer, B. L., and Cohen, R. C.: An atmospheric constraint on the NO$_2$ dependence of daytime near-surface nitrous acid (HONO), Environ. Sci. Technol., in revision, 2015.

Rood, M. J., Shaw, M. A., Larson, T. V., and Covert, D. S.: Ubiquitous nature of ambient metastable aerosol, Nature, 337, 537–539, 1989.

Russell, A. R., Valin, L. C., Bucsela, E. J., Wenig, M. O., and Cohen, R. C.: Space-based constraints on spatial and temporal patterns of NO$_x$ emissions in California, 2005–2008, Environ. Sci. Technol., 44, 3608–3615, doi:10.1021/es903451j, 2010.

Russell, A. R., Perring, A. E., Valin, L. C., Bucsela, E. J., Browne, E. C., Wooldridge, P. J., and Cohen, R. C.: A high spatial resolution retrieval of NO$_2$ column densities from OMI: method and evaluation, Atmos. Chem. Phys., 11, 8543–8554, doi:10.5194/acp-11-8543-2011, 2011.

Russell, A. R., Valin, L. C., and Cohen, R. C.: Trends in OMI NO$_2$ observations over the United States: effects of emission control technology and the economic recession, Atmos. Chem. Phys., 12, 12197–12209, doi:10.5194/acp-12-12197-2012, 2012.

Schiferl, L. D., Heald, C. L., Nowak, J. B., Holloway, J. S., Neuman, J. A., Bahreini, R., Pollack, I. B., Ryerson, T. B., Wiedinmyer, C., and Murphy, J. G.: An investigation of ammonia and inorganic particulate matter in California during the CalNex campaign, J. Geophys. Res.-Atmos., 119, 1883–1902, doi:10.1002/2013jd020765, 2014.

Sehmel, G. A.: Particle and gas dry deposition: a review, Atmos. Environ., 14, 983–1011, doi:10.1016/0004-6981(80)90031-1, 1980.

Shaw, S. L., Mitloehner, F. M., Jackson, W., Depeters, E. J., Fadel, J. G., Robinson, P. H., Holzinger, R., and Goldstein, A. H.: Volatile organic compound emissions from dairy cows and their waste as measured by proton-transfer-reaction mass spectrometry, Environ. Sci. Technol., 41, 1310–1316, doi:10.1021/es061475e, 2007.

Shaw Jr., R. W., Stevens, R. K., Bowermaster, J., Tesch, J. W., and Tew, E.: Measurements of atmospheric nitrate and nitric acid: the denuder difference experiment, Atmos. Environ., 16, 845–853, doi:10.1016/0004-6981(82)90403-6, 1982.

Sievering, H., Kelly, T., McConville, G., Seibold, C., and Turnipseed, A.: Nitric acid dry deposition to conifer forests: niwot ridge spruce-fir-pine study, Atmos. Environ., 35, 3851–3859, doi:10.1016/S1352-2310(01)00156-X, 2001.

Slinn, W. G. N.: Predictions for particle deposition to vegetative canopies, Atmos. Environ., 16, 1785–1794, doi:10.1016/0004-6981(82)90271-2, 1982.

Stolzenburg, M. R., Dutcher, D. D., Kirby, B. W., and Hering, S. V.: Automated measurement of the size and concentration of airborne particulate nitrate, Aerosol Sci. Tech., 37, 537–546, doi:10.1080/02786820300922, 2003.

Stull, R. B.: An Introduction to Boundary Layer Meteorology, 1st edn., Atmospheric and Oceanographic Sciences Library, vol. 13, Springer, the Netherlands, Kluwer Academic Publishers, London, UK, 1988.

Stutz, J., Alicke, B., Ackermann, R., Geyer, A., Wang, S. H., White, A. B., Williams, E. J., Spicer, C. W., and Fast, J. D.: Relative humidity dependence of HONO chemistry in urban areas, J. Geophys. Res.-Atmos., 109, D03307, doi:10.1029/2003jd004135, 2004.

Thornton, J. A., Wooldridge, P. J., and Cohen, R. C.: Atmospheric NO_2: in situ laser-induced fluorescence detection at parts per trillion mixing ratios, Anal. Chem., 72, 528–539, doi:10.1021/ac9908905, 1999.

Vayenas, D. V., Takahama, S., Davidson, C. I., and Pandis, S. N.: Simulation of the thermodynamics and removal processes in the sulfate-ammonia-nitric acid system during

winter: implications for $PM_{2.5}$ control strategies, J. Geophys. Res.-Atmos., 110, D07S14, doi:10.1029/2004JD005038, 2005.

Volpe Horii, C., William Munger, J., Wofsy, S. C., Zahniser, M., Nelson, D., and Barry Mc-Manus, J.: Atmospheric reactive nitrogen concentration and flux budgets at a Northeastern US forest site, Agr. Forest Meteorol., 133, 210–225, doi:10.1016/j.agrformet.2004.08.009, 2005.

Wagner, N. L., Riedel, T. P., Young, C. J., Bahreini, R., Brock, C. A., Dube, W. P., Kim, S., Middlebrook, A. M., Ozturk, F., Roberts, J. M., Russo, R., Sive, B., Swarthout, R., Thornton, J. A., VandenBoer, T. C., Zhou, Y., and Brown, S. S.: N_2O_5 uptake coefficients and nocturnal NO_2 removal rates determined from ambient wintertime measurements, J. Geophys. Res.-Atmos., 118, 9331–9350, doi:10.1002/jgrd.50653, 2013.

Waldman, J. M., Munger, J. W., Jacob, D. J., Flagan, R. C., Morgan, J. J., and Hoffmann, M. R.: Chemical-composition of acid fog, Science, 218, 677–680, doi:10.1126/science.218.4573.677, 1982.

Walker, J. M., Philip, S., Martin, R. V., and Seinfeld, J. H.: Simulation of nitrate, sulfate, and ammonium aerosols over the United States, Atmos. Chem. Phys., 12, 11213–11227, doi:10.5194/acp-12-11213-2012, 2012.

Watson, J. G., Chow, J. C., Bowen, J. L., Lowenthal, D. H., Hering, S., Ouchida, P., and Oslund, W.: Air quality measurements from the Fresno Supersite, J. Air Waste Manage., 50, 1321–1334, doi:10.1080/10473289.2000.10464184, 2000.

Weibring, P., Richter, D., Fried, A., Walega, J. G., and Dyroff, C.: Ultra-high-precision mid-IR spectrometer II: system description and spectroscopic performance, Appl. Phys. B-Lasers O., 85, 207–218, doi:10.1007/s00340-006-2300-4, 2006.

Weibring, P., Richter, D., Walega, J. G., and Fried, A.: First demonstration of a high performance difference frequency spectrometer on airborne platforms, Opt. Express, 15, 13476–13495, doi:10.1364/OE.15.013476, 2007.

Williams, E. J., Baumann, K., Roberts, J. M., Bertman, S. B., Norton, R. B., Fehsenfeld, F. C., Springston, S. R., Nunnermacker, L. J., Newman, L., Olszyna, K., Meagher, J., Hartsell, B., Edgerton, E., Pearson, J. R., and Rodgers, M. O.: Intercomparison of ground-based NO_y measurement techniques, J. Geophys. Res.-Atmos., 103, 22261–22280, doi:10.1029/98JD00074, 1998.

NO_x control over ammonium nitrate

S. E. Pusede et al.

Title Page

Abstract	Introduction
Conclusions	References
Tables	Figures

◀◀   ▶▶

◀   ▶

Back   Close

Full Screen / Esc

Printer-friendly Version

Interactive Discussion

Winer, A. M., Peters, J. W., Smith, J. P., and Pitts, J. N.: Response of commercial chemilu-minescent nitric oxide-nitrogen dioxide analyzers to other nitrogen-containing compounds, Environ. Sci. Technol., 8, 1118–1121, doi:10.1021/es60098a004, 1974.

Wooldridge, P. J., Perring, A. E., Bertram, T. H., Flocke, F. M., Roberts, J. M., Singh, H. B., Huey, L. G., Thornton, J. A., Wolfe, G. M., Murphy, J. G., Fry, J. L., Rollins, A. W., LaFranchi, B. W., and Cohen, R. C.: Total Peroxy Nitrates ($\sum$ PNs) in the atmosphere: the Thermal Dissociation-Laser Induced Fluorescence (TD-LIF) technique and comparisons to speciated PAN measurements, Atmos. Meas. Tech., 3, 593–607, doi:10.5194/amt-3-593-2010, 2010.

Zhang, J., Chameides, W. L., Weber, R., Cass, G., Orsini, D., Edgerton, E., Jongejan, P., and Slanina, J.: An evaluation of the thermodynamic equilibrium assumption for fine particulate composition: nitrate and ammonium during the 1999 Atlanta Supersite Experiment, J. Geophys. Res., 108, 8414, doi:10.1029/2001JD001592, 2003.

Zhang, Y., Liu, P., Liu, X.-H., Pun, B., Seigneur, C., Jacobson, M. Z., and Wang, W.-X.: Fine scale modeling of wintertime aerosol mass, number, and size distributions in central Califor-nia, J. Geophys. Res.-Atmos., 115, D15207, doi:10.1029/2009jd012950, 2010.

Title Page

Abstract | Introduction

Conclusions | References

Tables | Figures

◄ | ►

◄ | ►

Back | Close

Full Screen / Esc

Printer-friendly Version

Interactive Discussion

Table 1. Effects of three NO$_x$ emission control scenarios on wintertime 24 h PM$_{2.5}$q NAAQS exceedances in Fresno, Visalia, and Bakersfield. Rows 1–2: Average exceedances winter^{-1} (November–March) in the last 3 years of the record, rounded up and for which data exist, and percentage of days in violation. Rows 3–9: Number of exceedances predicted after a 50 % increase (back in time) and 50 and 75 % reductions in NO$_x$, including the calculated percent change from present day. In row 3, the number in parentheses is the actual number of exceedances averaged for 2001–2004.

Control	Fresno	Visalia	Bakersfield
exceedances (winter^{-1})	34	21	34
winter days in exceedance (%)	31	14	23
+50 % NO$_x$			
exceedances after the control (winter^{-1})	44 (60)	27 (31)	38 (53)
% change in exceedances	30	29	12
% change explained by the NO$_x$ reduction	39	60	22
−50 % NO$_x$			
exceedances after the control (winter^{-1})	30	19	27
% change in exceedances	−12	−10	−21
−75 % NO$_x$			
exceedances after the control (winter^{-1})	24	15	23
% change in exceedances	−30	−29	−33

Table A1. Species, measurement accuracy, analytical technique, time resolution, location/platform, and reference for select DISCOVER-AQ observation included in our analysis. Many compounds are measured with higher precision than accuracy. See original references for details.

Species	Accuracy (± %)	Analytical technique	Resolution	Location	Reference(s)
$NO_{3\,(g+p)}^-$	20	TD-LIF	1 s	P-3B	Day et al. (2002)
PM$_1$ ions	20	AMS	20 min	Fresno-Garland	Drewnick et al. (2005); Ge et al. (2012)
PM$_{2.5}$ ions	20	PILS	20 min	Fresno-Garland	
NO$_2$	5	LIF	1 s	P-3B	Thornton et al. (1999)
NH$_3$	35	cavity ring down	8–20 s	P-3B	Picarro G2103 analyzer
CH$_2$O	4	IR absorption	1 s	P-3B	Weibring et al. (2006, 2007)
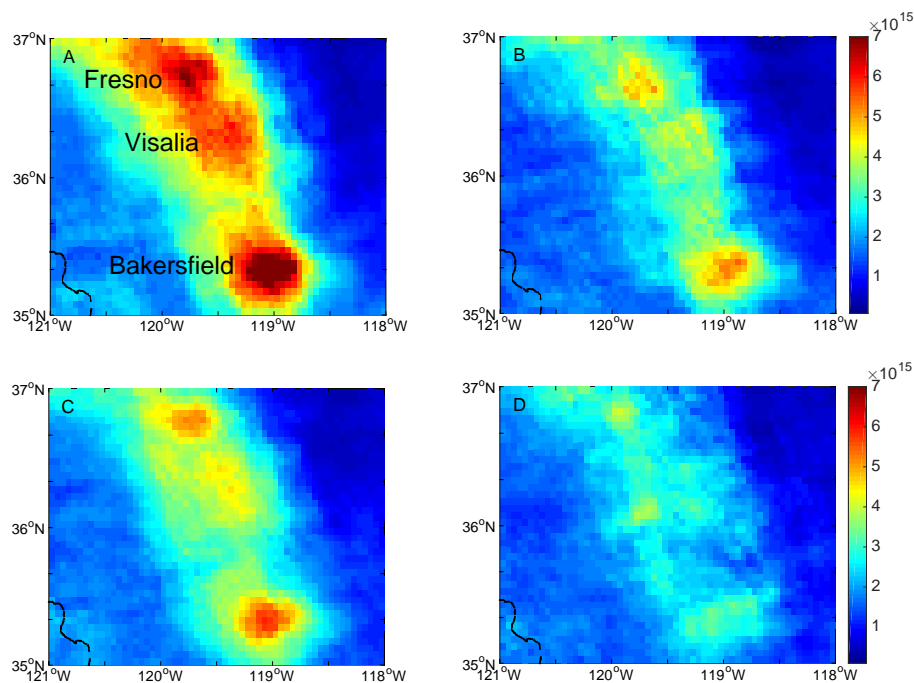
Figure 1. Wintertime (November–March) NO$_2$ columns (molecules cm^{-2}) in the SJV using the UC Berkeley OMI BEHR retrieval (Russell et al., 2011). The urban NO$_2$ plumes of Fresno, Visalia, and Bakersfield are labeled to the left of their respective cities in panel **(a)**. **(a)** 2005–2006 weekdays (Tuesday–Friday). **(b)** 2005–2006 weekends (Saturday–Sunday). **(c)** 2012–2013 weekdays. **(d)** 2012–2013 weekends.

Discussion Paper | Discussion Paper | Discussion Paper | Discussion Paper |

ACPD

15, 27087–27136, 2015

NO$_x$ control over ammonium nitrate

S. E. Pusede et al.

Title Page

Abstract | Introduction

Conclusions | References

Tables | Figures

|◄ | ►|

◄ | ►

Back | Close

Full Screen / Esc

Printer-friendly Version

Interactive Discussion
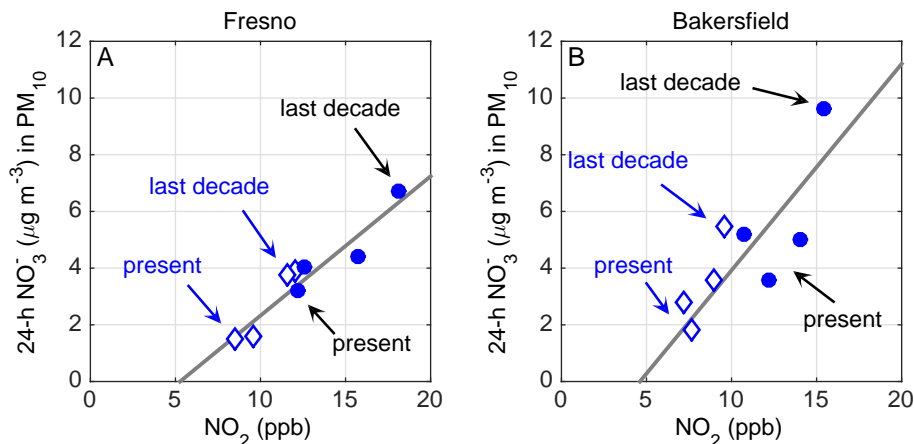
Figure 2. Observed NO_3^- ($\mu g\,m^{-3}$) vs. daytime (10 a.m.–3 p.m. LT) NO_2 on weekdays (closed circles) and weekends (open diamonds). Data are 3 year medians of wintertime (November–March) data in Fresno **(a)** (2001–2012) and Bakersfield **(b)** (2001–2013). There are an average of 41 weekday days and 18 weekend days point^{-1}. Uncertainties in NO_3^- are $\mu g\,m^{-3}$ on weekdays and $\mu g\,m^{-3}$ on weekends for NO_3^- and less than ±9 % on weekdays and ±13 % on weekends for NO_2 (see text for details). Slopes are 0.5 $\mu g\,m^{-3}\,NO_3^-\,ppb^{-1}\,NO_2$ in Fresno and 0.64 $\mu g\,m^{-3}\,NO_3^-\,ppb^{-1}\,NO_2$ in Bakersfield are calculated using a weighted linear least squares fit with errors assumed in both the x and y; weights are computed as counting errors derived from the number of observations.

Title Page

Abstract | Introduction

Conclusions | References

Tables | Figures

|◄ | ►|

◄ | ►

Back | Close

Full Screen / Esc

Printer-friendly Version

Interactive Discussion
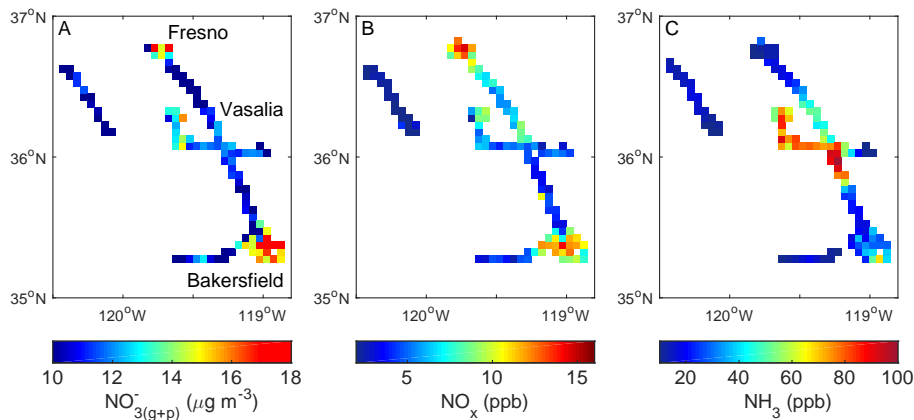
Figure 3. $NO_{3(g+p)}^{-}$ ($\mu g\,m^{-3}$) **(a)**, NO_x (ppb) **(b)**, and NH_3 (ppb) **(c)** measured onboard the NASA P-3B below the fully formed afternoon boundary layer on the same days averaged to a $0.05° \times 0.05°$ grid.

free troposphere

nocturnal boundary layer (NBL)
$NO + O_3 \rightarrow NO_2$
if $O_3 = 0$,
then $PNO_3^-{}_{(p)} = 0$

daytime boundary layer
$NO_2 + OH \rightarrow HNO_3$

nocturnal boundary layer (NBL)
$NO_2 + O_3 \rightarrow NO_3$
$NO_3 + NO_2 \rightarrow \rightarrow 2NO_3^-{}_{(p)}$

NH_4NO_3 produced in the NRL is mixed into the boundary layer in the morning

surface monitor

sunrise   sunset
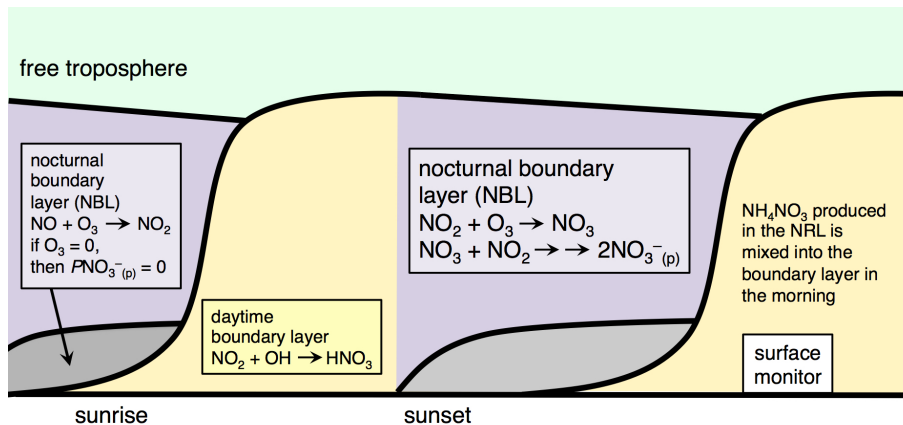
Figure 4. Simplified illustration of the diurnal evolution of the near-surface atmosphere as it relates to PNO_3^-. Boundary layer dynamics schematic adapted from Stull (1988).
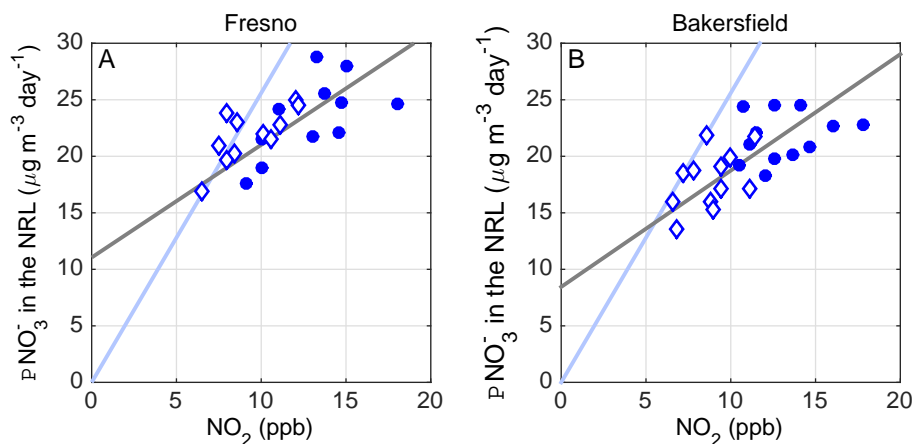
Figure 5. Calculated wintertime median PNO$_3^-$ (μg m^{-3} day^{-1}) in the NRL vs. daytime (10 a.m.–3 p.m. LT) NO$_2$ (ppb) on weekdays (closed circles) and weekends (open diamonds) in Fresno **(a)** for each year in 2001–2012 and in Bakersfield **(b)** in 2001–2013 (blue). The light blue line has a slope of 2.56, expected for unit conversion of NO$_2$ to NO$_3^-$ (ppb to μg m^{-3}). The actual NO$_3^-$ vs. NO$_2$ slope (gray line) is calculated using a weighted linear least squares fit with errors assumed in both the x and y and weights that are the counting errors derived from the number of observations. Time follows the NO$_2$ trend.
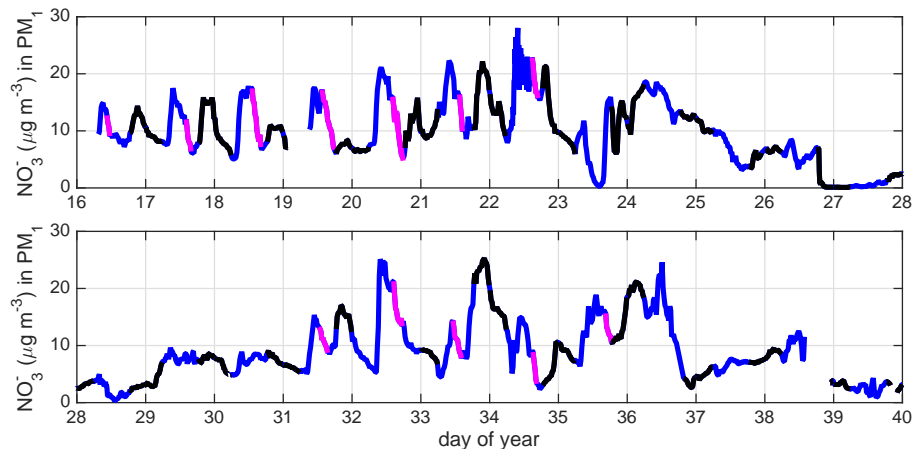
Figure 6. Time series of NO$_3^-$ (μg m^{-3}) measured at the ground in Fresno during DISCOVER-AQ. Days are in blue and nights are in black. Select afternoon data (magenta) were fit to derive $\tau_{NO_3^-}$.
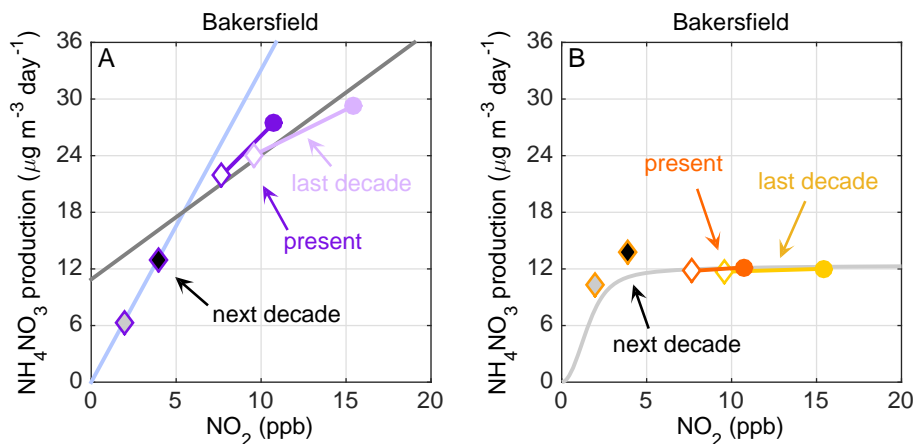
Figure 7. In Bakersfield, tethered 3 year weekday (closed circles) and weekend (open diamonds) medians of calculated wintertime NH_4NO_3 production ($\mu g\,m^{-3}\,day^{-1}$) in the NRL **(a)** and during the daytime **(b)** vs. NO_2. Brighter data are observationally-constrained 3 year medians at present (2010–2013). Pale points are observationally-constrained 3 year medians at the start of the record (2001–2004). Predicted NH_4NO_3 production at –50 % weekend NO_x are black-filled diamonds and –75 % weekend NO_x are gray-filled diamonds. Weekend data were selected simply to expand the NO_x range of individual curves; impacts on weekdays can be inferred. In panel **(a)** the light blue line is stoichiometric and the gray line is a fit to the annual observations as in Fig. 5. In panel **(b)** the gray line is the calculated HNO_3 production with PHO_x and organic reactivity equal to present-day values.

Title Page

Abstract | Introduction

Conclusions | References

Tables | Figures

|◄ | ►|

◄ | ►

Back | Close

Full Screen / Esc

Printer-friendly Version

Interactive Discussion
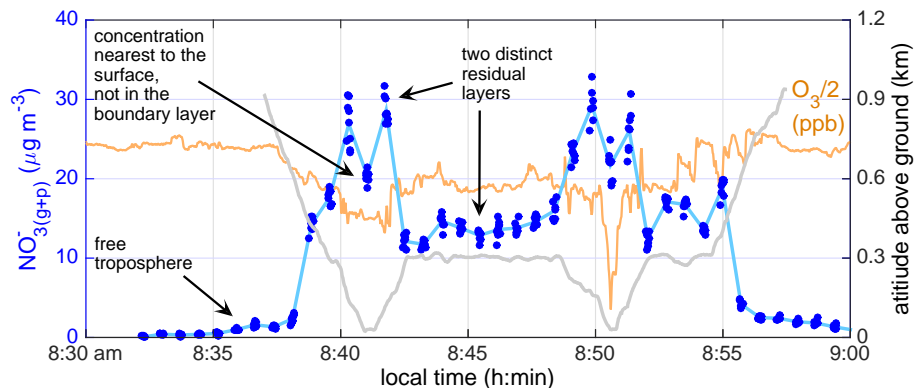
Figure A1. Vertically resolved $NO_{3\,(g+p)}^-$ (blue) during a morning DISCOVER-AQ flight segment. The O_3 data (ppb/2) (orange) are associated with the left-hand axis. The altitude above ground (gray) is shown on the right-hand axis.

Full Screen / Esc

Printer-friendly Version

Interactive Discussion
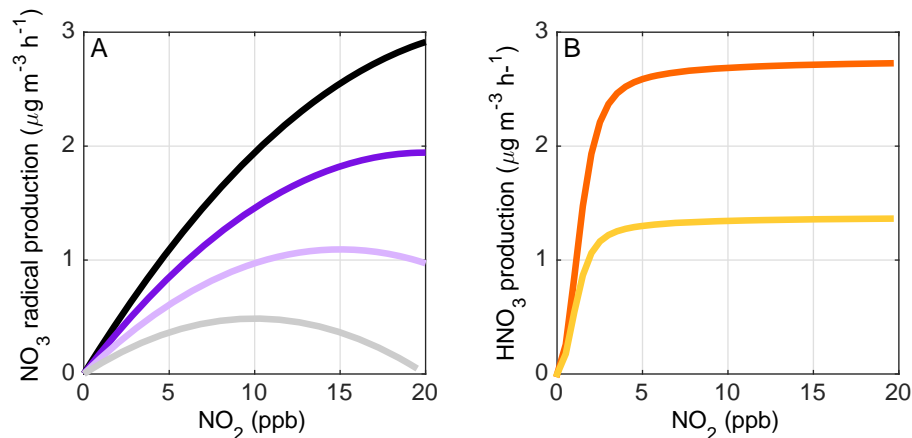
Figure B1. (a) NO$_3$ radical production (µg m^{-3} h^{-1}) vs. NO$_2$ (ppb) under four O$_x$ conditions: 50 ppb O$_x$ (black), 40 ppb O$_x$ (purple), 30 ppb O$_x$ (violet), and 20 ppb O$_x$ (gray). The temperature is 282 K. **(b)** Production of HNO$_3$ (µg m^{-3} h^{-1}) as a function of NO$_2$ computed with an analytical model at NO : NO$_x$ = 0.3 and VOCR = 4 s^{-1} at 0.3 ppt s^{-1} PHO$_x$ (orange) and 0.15 ppt s^{-1} PHO$_x$ (golden).
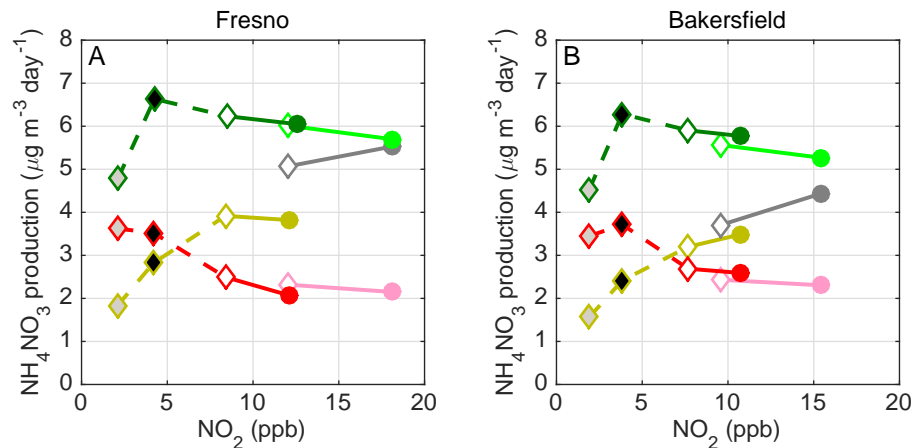
Figure B2. Wintertime $NH_4NO_3^-$ production ($\mu g\,m^{-3}\,day^{-1}$) by OH-initiated chemistry vs. daytime (10 a.m.–3 p.m. LT) NO_2 (ppb) for each individual HO_x precursor: $O(^1D)+H_2O$ (red), HONO (yellow), and CH_2O (green). Data are tethered present-day 3 year medians on weekdays (closed circles) and weekends (open diamonds) in Fresno **(a)** and Bakersfield **(b)**. Lighter tint data are tethered 3 year medians at the start of the record (2000–2003). Predicted $NH_4NO_3^-$ production calculated at −50 % weekend NO_x (NO_x black-filled diamond) and −75 % weekend NO_x (gray-filled diamond) are also shown.
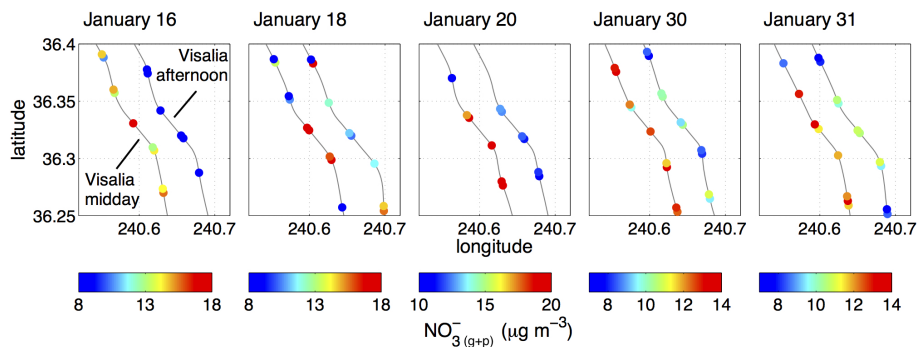
Figure C1. NO$_{3\,(g+p)}^{-}$ (μg m^{-3}) measured during ten missed approaches on five days over Visalia. The left-hand flight track is the midday (12–1 p.m. LT) missed approach and the right-hand track, shifted east by 0.02°, is the afternoon (3–4 p.m. LT) missed approach.